Planetary and Space Science 193 (2020) 105091

Contents lists available at ScienceDirect

Planetary and Space Science

journal homepage: www.elsevier.com/locate/pss

Basaltic fissure types on Earth: Suitable analogs to evaluate the origins of volcanic terrains on the Moon and Mars?

Scott S. Hughes [a,*], W. Brent Garry [b], Alexander Sehlke [c,d], Eric H. Christiansen [e], Shannon E. Kobs Nawotniak [a], Derek W.G. Sears [c,d], Richard C. Elphic [c], Darlene S.S. Lim [c], Jennifer L. Heldmann [c]

[a] Department of Geosciences, Idaho State University, Pocatello, ID, 83209, USA
[b] NASA Goddard Space Flight Center, Geology, Geophysics and Geochemistry Lab, Greenbelt, MD, 20771, USA
[c] NASA Ames Research Center, Mountain View, CA, 94035, USA
[d] Bay Area Environmental Research Institute, Petaluma, CA, 94952, USA
[e] Department of Geological Sciences, Brigham Young University, Provo, UT, 84602, USA

ARTICLE INFO

Keywords:
Basalt
Volcanic fissure
Moon
Mars
Earth analogs

ABSTRACT

Basaltic eruptive fissures of the Great Rift and surroundings on the eastern Snake River Plain of Idaho, USA, and selected volcanic features in Hawai'i, Iceland and northern Africa were surveyed for their relevancy as planetary analogs. Evaluated during field investigations and in satellite imagery for structures, physiography, and geologic setting, fissures were categorized into four broad types: (1) simple, monogenetic fissures with obvious volcanic constructs or deposits, (2) monogenetic fissures now obscured by low shields or relatively large cones, (3) polygenetic volcanic rift zones with multiple vents and deposits, and (4) compound regional fissure systems or dike swarms that comprise major rift zones or large volcanic terrains. Using this classification as an initial base, we surveyed imagery of volcanic features for likely fissure vents in two major geologic settings **on the Moon**: floor-fractured craters (FFCs) and mare and cryptomare provinces. Two major regions on Mars, the volcanic plains around Alba Mons and the greater Tharsis region, were also surveyed for fissure types and volcanic associations of fissure-like features. The planetary surveys suggest that the proposed classification provides a suitable analog starting point to interpret structures associated with fissure systems on the Moon and Mars.

With few exceptions, our survey indicates that each of the studied terrains exhibits a dominant fissure type. Type 1 fissures, most with pyroclastic deposits, prevail in lunar FFCs and mare-like regions; whereas type 2 fissures are ubiquitous in the Tharsis region of Mars and a few exist on the Moon as low shields. Type 3 volcanic rift zones are not common on either the Moon or Mars, although they might become evident in future work on chemically evolved terrains. Type 4 fissures are inferred in mare terrains, often represented as the extensions of major linear rille networks or rimae, with possibly complex dike swarms that were buried beneath voluminous mare basalt lava flows. Likewise, numerous flood lavas on Mars are possibly associated with now-obscured or difficult to define type 4 fissure systems.

1. Introduction

Linear or curvilinear eruptive fissures, the surface expressions of steeply-dipping pressurized feeder dikes, are the dominant volcanic vents through which relatively low viscosity basaltic magma reaches the surface of a planet. Fissures, usually transient features in the growth of lava terrains, are the sources for pyroclastic ejecta, low-volume proximal lava flows, and high-volume lava flows that stretch for many kilometers. They occur in many geologic settings: rift zones with lava-filled depressions and grabens, large mafic shield volcanoes covered by numerous thin lava flows, lava plains comprising coalesced low shields, and vast regions covered by thick sequences of flood basalt. These volcanic terrains and their variants portray crustal extension due to magmatic or tectonic forces, or both, and some of them ultimately develop landscapes characterized by sub-parallel fissures. While recent studies have focused on interpreting equivalent processes on currently inaccessible planetary

* Corresponding author.
E-mail address: hughscot@isu.edu (S.S. Hughes).

https://doi.org/10.1016/j.pss.2020.105091
Received 18 January 2020; Received in revised form 29 August 2020; Accepted 11 September 2020
Available online 15 September 2020

terrains, there is a need to demonstrate the similarities of Earth analogs to planetary fissure systems, although surficial features or geologic settings often are somewhat different (e.g., Carr, 1973; Greeley and King, 1977; Greeley and Schultz, 1977; Moore and Hodges, 1980; Wilson and Head, 1994; Hodges and Moore, 1994; Spudis, 1999; Plescia, 2004; Hauber et al., 2009; Head and Wilson, 2017).

In order to classify volcanic fissures on Earth as planetary terrains, we evaluate relatively young features of the Great Rift and surroundings on the eastern Snake River Plain (ESRP) of Idaho, USA, and selected features in Hawai'i, Iceland, and northern Africa. Physiography examined in the field and in aerial imagery is used to categorize fissures associated with volcanism on Earth, which can then be compared as analogs to volcanic features on other planetary bodies. The intention of this study is to elucidate the association of fissure-related structures in two volcanic terrains on the Moon: lunar floor-fractured craters (FFCs), and lunar mare and cryptomare basalts. We extend this comparative study to the volcanic plains in the greater Tharsis region of Mars. *The leading question here is whether or not the categorized fissure types on Earth are suitable analogs for broadly similar features in these terrains*.

Fissure eruptions were likely dominant features during the growth of all three volcanic terrains discussed here; yet, this hypothesis may be difficult to test with currently available data. The classification of similar types using analogs also depends on recognizing how landforms develop in geologic settings that differ from those on Earth. Differences in gravity, atmospheres (or lack of), and planetary interiors (crust-mantle compositions and thicknesses, tectonism, thermal structures, etc.), can account for overall differences in morphology and morphometry of volcanic features. These factors are treated in comprehensive models of magma ascent, emplacement, and eruption on both the Moon (Head and Wilson, 2017) and Mars (Wilson and Head, 1994), with detailed consideration of known or theoretical conditions related to the development of volcanic features, deposits, and structures. For example, compared to Earth, the lower gravity and atmospheric pressure of either Mars or the Moon will cause gas-driven eruptions (typical of basaltic systems) to initiate at greater depths of gas exsolution and magma disruption. Moreover, compared to Earth, both the Moon and Mars will have broader dispersal of pyroclastic ejecta and lava fields, as well as lower relief volcanic constructs.

We hypothesize that while fissure systems on any planetary body may be similar at a fundamental level, differences will become apparent at complex levels due to the presence (or lack) of some distinctive associated features. A secondary issue, therefore, is how broadly each type of fissure system must be defined in order to be considered a suitable planetary analog. Volcanism on the Moon and on Mars, most of which occurred early in their geologic histories, is manifested on both bodies in generally dissimilar patterns (e.g., Carr, 1973; Neal and Taylor, 1992; Hodges and Moore, 1994; Wilson and Head, 1994; Spudis, 1999; Carr and Head, 2010; Head and Wilson, 2017, and many others). One of the primary morphological differences is that most vents related to the prodigious lunar mare basalts and martian lava plains are likely buried beneath lava flows, yet on Mars many vents, cones and flows remain visible.

Although recent high-resolution orbital platforms have enhanced our views of the Moon, no attempt is made here to reclassify or revise the interpretations derived from surface features or analyzed samples in many previous studies (e.g., Schultz, 1976; Wilson and Head, 1981, 2018a; Head and Wilson, 1992, 2017; Jolliff et al., 2000; Plescia, 2004; Shearer et al., 2006; Wilson et al., 2011; Hurwitz et al., 2013; Spudis et al., 2013; Jozwiak et al., 2012, 2015, 2017). Instead, this survey of fissure vents and volcanic features on the Moon focuses on determining the similarities and differences among them and how they are related to analogs on Earth. Morphometric assessment of lunar vents in both FFC and mare settings is used to quantify such associations with the intent to improve the understanding of magmatic processes, whether observed or implied.

A slightly different approach is used to evaluate volcanic fissures on Mars, mainly because of the difference in available imagery and the current knowledge of specific, albeit significant, volcanic landforms. While a variety of volcanic features on Mars have been extensively studied on the main volcanic edifices and lava plains (e.g., Hodges, 1979; Hodges and Moore, 1994; Wilson and Head, 1994, 2002; Moore and Hodges, 1980; Scott et al., 2002; Mège et al., 2003; Wyrick et al., 2004; Bleacher et al., 2009; Hauber et al., 2009, 2011; Wilson et al., 2009; Brož and Hauber, 2013; Bamberg et al., 2014; Henderson et al., 2015; Richardson et al., 2017; Peters and Christiansen, 2017), we focus on potential fissure vents around Alba Mons and low shields on the flanks of major Tharsis shields. This comparison follows the premise that basaltic fissures may have manifested in various forms on other planetary bodies even if the visible evidence has been degraded over time.

Thus, a selected subset of key visible landforms on Mars is presented, rather than attempting to include all of the many volcanic landforms, with the intent to broadly outline their distinction from volcanic systems on the Moon. One important consideration is eruptive environment, especially gravity, atmospheric and subsurface hydrologic influences compared to the Moon (Wilson and Head, 1994; Head and Wilson, 2017). We purposely avoided landforms such as tuff rings that represent basaltic eruptions influenced by water reservoirs or permafrost although they represent significant volcanic processes on Mars (e.g., Brož and Hauber, 2013). Moreover, we briefly address FFCs on Mars, another significant landform (Bamberg et al., 2014), but without detailed assessment mainly because they have not been analyzed and modeled in as much detail as the FFCs on the Moon (e.g., Jozwiak et al., 2012, 2015; 2017; Wilson and Head, 2018), nor does available imagery reveal fissure vents with sufficient resolution. Both of these volcanic landforms on Mars deserve a more comprehensive assessment, including comparative analyses, in future studies.

1.1. Methods

Relatively young and unaltered volcanic features on the Great Rift and surrounding regions of the eastern Snake River Plain (ESRP) of Idaho, USA (Fig. 1) were selected on the basis of extensive previous work (Greeley and King, 1977; Kuntz et al., 1992, 2007; Hughes et al., 1999), our own 2014–2018 field investigations (e.g., Sears et al., 2017; Hughes et al., 2018, 2019), and visibility using Google Earth (Landsat/Copernicus, ©2019 Google LLC) imagery. These features are excellent analogs and the original basis for plains volcanism responsible for lava terrains on planetary surfaces (Greeley, 1982). Additional information is derived from fissure systems of Hawai'i, Iceland and the East Africa Rift to round out representative styles in various geologic settings and demonstrate the utility of currently available exploration tools. Examples of basaltic fissure vents on Earth (Table 1) are based solely on satellite imagery using the criteria of minimal degradation and the appearance of being a relatively young feature in a regional volcanic field. Additional weight is given to systems where the fissure length, fissure orientation and/or overall extent of fresh volcanic deposits can be mapped (or estimated) using remote sensing.

The primary source of information for Table 1 is the Smithsonian Institution's volcano database (Global Volcanism Program, 2013), which lists 1433 volcanoes active during the Holocene (10,000 years CE to present) and 1239 volcanoes of Pleistocene age. Some pre-Holocene volcanoes that erupted during latest Pleistocene appear relatively fresh, including three ESRP representatives: Cerro Grande, North Robbers, and South Robbers (Kuntz et al., 1992; Hughes et al., 1999). Information provided in Table 1, including any necessary refinements in location, fissure lengths, and associated structures, additionally derives from Landsat imagery (Google Earth) as well as other referenced sources.

Eruptive and non-eruptive fissures and their related volcanic structures on the Moon and Mars, except for those investigated during lunar Apollo crewed and Mars rover missions, are examined remotely using presently available images. Lunar features are primarily examined using the Lunar Reconnaissance Orbiter Camera (LROC) in Quickmap

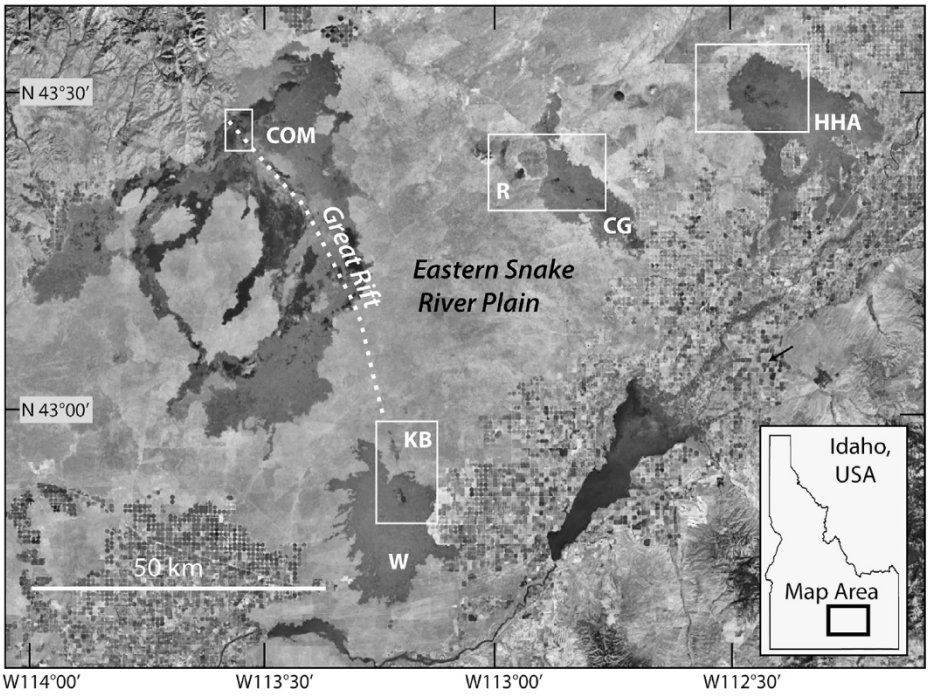

Fig. 1. Study region on the eastern Snake River Plain (ESRP). White boxes indicate regions of detail shown in Fig. 4. Map abbreviations for vents and lava fields are: COM = Craters of the Moon; KB = Kings Bowl; W = Wapi; R = Robbers (North and South Robbers); CG = Cerro Grande; HHA = Hells Half Acre. Map base is grayscale of Google Earth Landsat imagery.

Table 1
Selected latest Pleistocene – Recent basaltic fissure vents on Earth as analogs for planetary volcanism.

Name	Country/Region	Setting	Lat. (°)	Long. (°)	Length (km)[a]	Type	Ref.
Kings Bowl	Idaho, USA	ESRP	42.949	−113.216	6.1	1	2, 3
Great Rift	Idaho, USA	ESRP	43.444	−113.561	28	3	3, 4
Wapi (Pillar Bt)	Idaho, USA	ESRP	42.885	−113.215	?	2	1, 2, 3
N. Robbers	Idaho, USA	ESRP	46.381	−112.987	2.9	1	3, 4
S. Robbers	Idaho, USA	ESRP	43.358	−112.969	1.7	1	3, 4
Hells Half Acre	Idaho, USA	ESRP	43.489	−112.449	(7.2)	2	1, 3
Cerro Grande	Idaho, USA	ESRP	43.360	−112.878	(6.2)	2	3, 4
Hertali	Ethiopia	EAR	9.771	40.338	11	1	1, 5
Ardoukoba	Djibouti	EAR	11.602	42.462	3.9	3	1, 6
Alu-Dalaffilla	Ethiopia	EAR	13.793	40.553	83	3 (4)	1
Manda-Inakir	Ethiopia	EAR	12.384	42.219	43	4	1, 7, 8
Ljósufjöll	Iceland	ORZ	64.918	−22.588	26	3	1
Krafla	Iceland	ORZ	65.725	−16.793	4.9	1	1
Reykjanes (segment)	Iceland	ORZ	63.862	−22.526	4.5	4	1, 9
Nýjahraun	Iceland	ORZ	65.585	−16.420	13.6	1	1
Holuhraun	Iceland	ORZ	64.868	−16.837	1.5	1	1
Lakagigar (Laki)	Iceland	ORZ	64.073	−18.233	21	4	10
Kamoamoa	Hawai'i, USA	ERZ	19.375	−155.137	0.8	1	11
Pu'u 'O'o	Hawai'i, USA	ERZ	19.389	−155.106	11.9	2	11
Mauna Ulu	Hawai'i, USA	ERZ	19.367	−155.201	(4)	2	11
Mauna Iki	Hawai'i, USA	SWRZ	19.348	−155.355	8	1	12, 13
Red Cones S	Hawai'i, USA	SWRZ	19.248	−155.412	0.36	1	12
Pu'u U'aulu S	Hawai'i, USA	SWRZ	19.199	−155.431	0.46	1	12
Kamaka Hills	Hawai'i, USA	SWRZ	19.307	−155.364	3.2	1	12
Ka'u Desert 12/74	Hawai'i, USA	SWRZ	19.375	−155.297	4.1	1	12, 13

[a] Fissure lengths determined using Landsat imagery and Google Earth ® tools, estimated values in parentheses. Abbreviations for settings: ESRP = eastern Snake River Plain, EAR = East African Rift, ORZ = Oceanic Rift Zone, ERZ = East Rift Zone, SWRZ = Southwest Rift Zone. References: 1 – Global Volcanism Program (2013); 2 – Greeley and Schultz (1977); 3 – Kuntz et al. (1992); 4 – Hughes et al. (1999); 5 – Mohr and Wood (1976); 6 – Needham et al. (1976); 7 – Audin et al. (1990); 8 – Jenness and Clifton (2009); 9 – Thordarson and Self (1993); 10 – Orr et al. (2012); 11 – Wolfe and Morris (1996); 12 – Neal and Lockwood (2003).

(https://quickmap.lroc.asu.edu), a comprehensive georeferenced mapping system that features Wide Angle Camera (WAC) 100 m/pixel mosaic base maps and Narrow Angle Camera (NAC) 0.5 m/pixel images, Kaguya TC images, and overlays based on many available datasets from other lunar orbiters. The study of volcanic features on Mars relies on images derived from the Context Camera (CTX) on Mars Reconnaissance Orbiter (Malin et al., 2007). The images provide details over wide ~30 km swaths with high contrast and spatial resolution of ~ 5–6 m/pixel, attributes that make CTX well-suited for the study of relatively small volcanic features.

2. Basaltic fissures on Earth

The appearances of volcanic structures as landforms, especially smaller-sized features, are typically short-lived or diminished because subsequent eruptions often obscure the initial linear vents with fresh lava flows and pyroclastic ejecta. Even relatively young volcanic provinces with fresh-appearing lava flows may exhibit neither the original eruptive fissure(s) nor related structures simply because more recent volcanic activity has obliterated them. Nonetheless, analog eruptive fissures visible on Earth's surface are abundant and most often associated with active or recently active volcanic provinces.

Craters of the Moon (COM) lava field is one such province on the ESRP with fresh appearing examples of basaltic fissures depicted in various landforms. Lying on the northern segment of The Great Rift, COM and, on the southern segment, the Kings Bowl and Wapi lava fields (Fig. 1) together comprise the Craters of the Moon National Monument and Preserve. The preserve, as well as the surrounding ESRP, is a region of continental crustal extension that overprints the time-transgressive track of Miocene – Pliocene silicic eruptions related to the Yellowstone hotspot (Armstrong et al., 1975; Pierce and Morgan, 1992; Smith and Braile, 1994). Subsequent volcanism in the late Pleistocene and Holocene produced well-exposed planetary analogs, including volcanic rift zones and eruptive fissures in various stages of low shield growth (e.g., Greeley, 1982; Greeley and King, 1977; Kuntz et al., 1992; Hughes et al., 1999, 2002, 2018). Many of these were examined during 2014–2018 field excursions related to this study as well as many previous visits over the past three decades.

2.1. Structures related to volcanic fissures

Our basic principle is that the identification, interpretation and categorization of volcanic fissures on other planetary bodies depends on two overall requirements, one of which is understanding the volcanic processes that lead to observable structures. The other is that surficial evidence of a volcanic fissure used as an analog to categorize fissure types must include observable structures that can either be directly associated with a volcanic process or interpreted to infer a volcanic system. One or more linear or aligned components such as open fissures, dikes, extension cracks, grabens, spatter ramparts, explosion pits, collapse pits, and elongate vents or cones must be present. All of these surficial structures, typically representing dike injection, are manifested as surface features on the ESRP (e.g., Kuntz et al., 1992, 2002; Holmes et al., 2008; Hughes et al., 2018).

A relatively simple basaltic eruptive fissure with concomitant aligned structures is Kings Bowl, (Fig. 2, left), which is one of several prominent ESRP planetary analogs (Greeley and Schultz, 1977; Greeley et al., 1977). Features revealed by field investigations include spatter cones, spatter ramparts, lava ponds, lava outflow lobes, pyroclastic ejecta blocks, extension cracks, non-eruptive fissure segments, exposed dikes and more (e.g., Greeley and Schultz, 1977; Hughes et al., 1999, 2018). By comparison, an apparent volcanic feature in the Cyane Fossae region of Mars (Fig. 2, right) exhibits a few similar parallel structures. Structures evident in the CTX image, including a graben, extension cracks (flanking a central obscured fissure), and either explosion or collapse pits, are most likely related to arrested dike intrusion (e.g., Mège and Masson, 1996; Scott et al., 2002; Wilson and Head, 2002; Hughes et al., 2015).

Sketch maps of these two systems (Fig. 2) illustrate features that can be recognized in the available imagery. These maps, and those derived from subsequent investigations herein, depict how features are interpreted, or possibly misinterpreted, without ground-truth examination. Thus, the interpretations depend strongly on both the type of imagery and the ability to connect features to processes. Eruptive features such as lava flow lobes, vents or cones cannot be directly associated with the Cyane Fossae fissure; however, the aligned structures, as well as lava flow

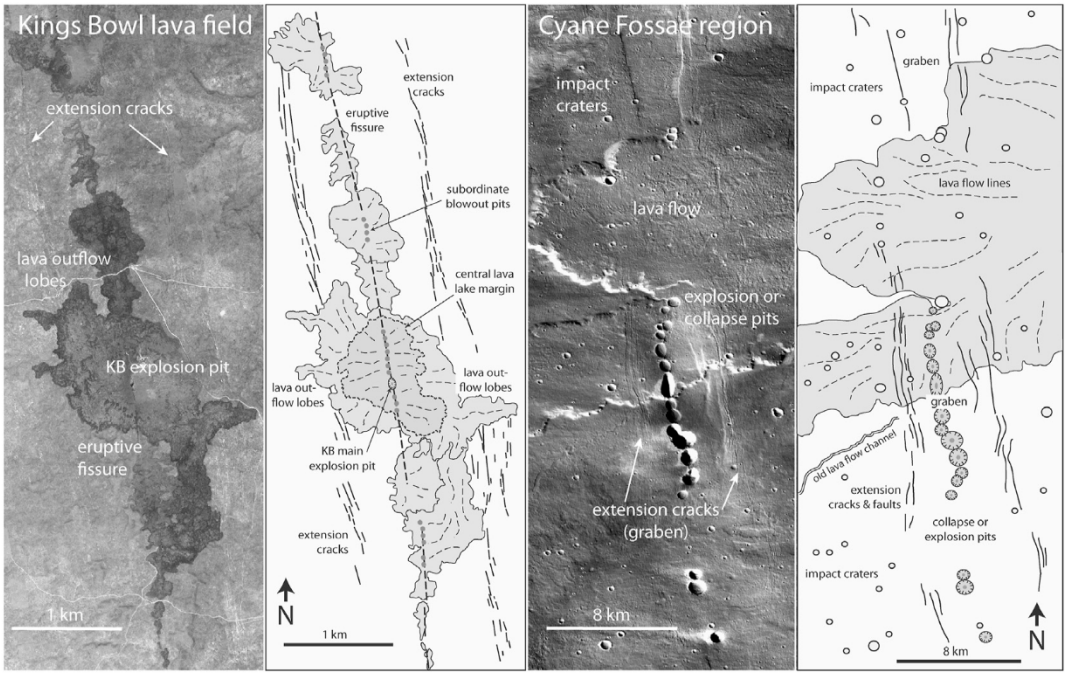

Fig. 2. Kings Bowl, on left (grayscale of Google Earth Landsat image and sketch map of salient features), is a relatively simple, short-lived en echelon eruptive fissure. The fissure eruption with phreatic explosion pits, extension cracks, dike-fed spatter ramparts and lava outflow lobes, illustrates typical planetary analog structures (e.g., Greeley and Schultz, 1977; Greeley et al., 1977; Kuntz et al., 1992, 2002; Hughes et al., 1999, 2018). A comparative non-eruptive feature located in the Cyane Fossae region of Mars, on right (CTX- P06_003515_2155_XI_35N120W image and sketch map) illustrates additional structures, e.g., grabens and pit craters that formed in a similar geologic setting and are partially buried by a thick, tabular lava flow. Except for some extension cracks and the lava lake in Kings Bowl field (mapped previously, e.g., Greeley et al., 1977; Holmes et al., 2008; Hughes et al., 2018), most features in each system are mapped according to visibility in available imagery without the benefit of detailed ground-level investigation. Labels indicate the most important features necessary to evaluate geologic processes relevant to fissure categorization.

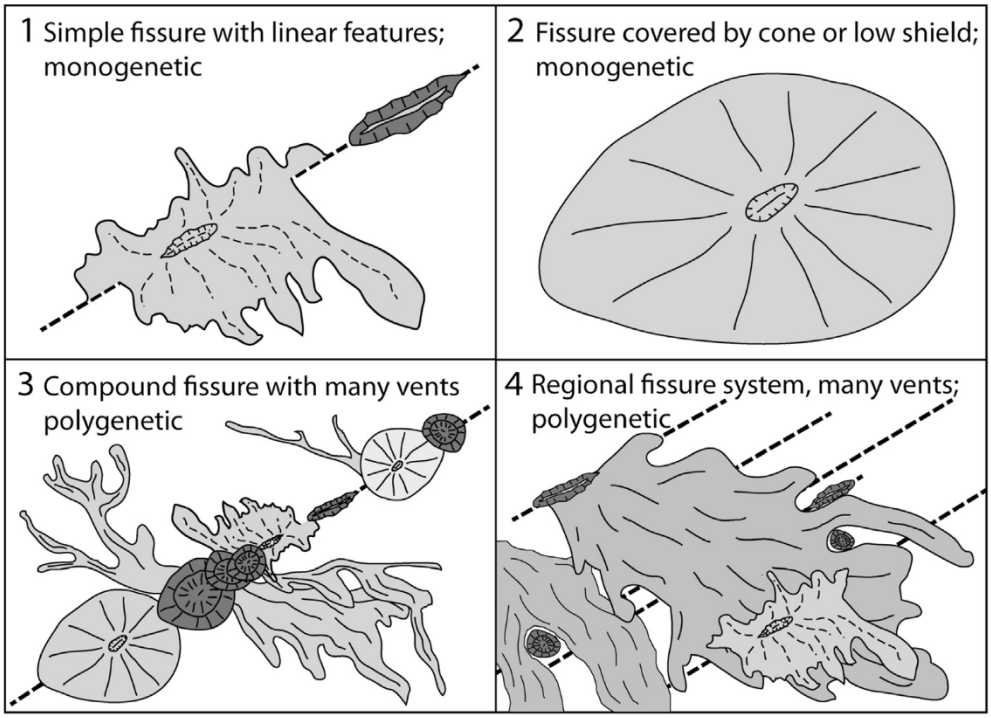

Fig. 3. Schematic illustration of basaltic fissure types (variable scales), categorized from Earth analogs. Volcanic features are depicted in various shades to illustrate different types of deposits (e.g., dark gray = spatter or cinder cone; lighter shades = lava flows or chemically evolved tephra). Types 1–3 are represented on the ESRP and many other volcanic provinces, while type 4 fissures are components of and associated only with large igneous provinces such as major mid-ocean ridge rift zones and continental flood basalts.

lobes (emplaced prior to and cut by graben formation), portray a simple system that is superficially similar to Kings Bowl. This analog comparison and others where surficial structures are not entirely equivalent helps determine the breadth of each category used in our classification system.

Surficial components of a fissure system thus provide important evidence for subsurface dynamic processes. Volcanic principles show that magma will rise to a level of neutral buoyancy (dictated mainly by surrounding lithostatic pressure, depth to a reservoir, and magma density), but the driving force for an eruption is dominantly gas expansion. Along a dike-induced fissure, structures such as extension cracks, grabens, and collapse pits reflect crustal stresses due to pressure equilibration at the top of the magma column as the dike is injected (e.g., Pollard et al., 1983; Mastin and Pollard, 1988; Rubin, 1992; Rubin and Pollard, 1988; Gudmundsson, 2003). In the example above (Fig. 2), the dimensions of volcanic features used to evaluate the eruption dynamics of Kings Bowl on Earth (Kuntz et al., 2002; Holmes et al., 2008; Hughes et al., 2018) facilitate a better understanding of non-eruptive systems such as Cyane Fossae on Mars. In a similar manner, surface features have also contributed to deriving comprehensive models of lunar magmatism (e.g., Wilson et al., 2011; Head and Wilson, 2017; Wilson and Head, 2018a).

2.2. Types of basaltic fissure systems

Categorization of fissure types is founded on the appearance of structures in a given fissure, as either simple (single) or multiple (often en echelon) features, and the apparent volcanic history. The terms "monogenetic" and "polygenetic" are used as part of this categorization. However, while these terms are common in terrestrial volcanic descriptions, they are not commonplace in the description of planetary deposits. Walker (2000) defines a monogenetic volcano as one that erupts only once; whereas, a polygenetic volcano erupts repeatedly, often in an episodic manner. This rudimentary definition suffices for many examples; yet, we recognize myriad variants and complexities, especially in alleged monogenetic systems, that we attempt to clarify where possible. We consider a single eruption to mean a single eruptive phase, whether or not multiple lava flows, eruptive vents, pyroclastic deposits or even magma sources are involved. A monogenetic eruptive phase may last a few hours to produce a single lava flow or pyroclastic deposit such as Kings Bowl on the ESRP, or last intermittently for a few decades to produce a low shield such as Pu'u 'Ō'ō in Hawai'i, or Rangitoto Island in New Zealand. We further use polygenetic to refer to long-term complex systems (hundreds to millions of years) such as the East Rift Zone of Kīlauea, Hawai'i, as well as to large individual volcanoes such Mauna Loa in Hawai'i and Mt. Fuji in Japan. Moreover, many polygenetic volcanic fields are made up of monogenetic eruptions.

Fissures in our observations (Fig. 3) can be defined in four types: (1) simple, monogenetic eruptive fissure with exposed linear features; (2) monogenetic eruptive fissure mostly or completely obscured by pyroclastic cone or lava shield; (3) compound polygenetic fissure with multiple vents; and (4) regional polygenetic system of fissures in a large igneous province. Each fissure type represents processes that likely occurred during fissure development, both visible and inferred, and the factors inherent to the geologic setting. Factors such as topography, regional stress field (either tectonic or magmatic), inferred lava properties and the complexity of the vent system are all considered in this assessment of fissure types.

For example, a sustained eruption that started out as a connected series of type 1 fissure vents may now be represented by a pyroclastic cone or low shield with or without a central vent. Flow directions of lava outflow lobes may reveal topographic control to help decipher the fissure orientation. Lateral subsurface migration of magma or a drop in magma supply may also cause drain-back leaving open cracks, empty vertical chambers or other linear features that extend some distance beyond the original eruptive fissure.

All four types are used here to express surface features related to geologic processes. Each one represents an analog to features that may be linked to the geologic settings and volcanic histories of the Moon, Mars and some smaller planetary bodies. An important consideration is the potential difference in scale as exemplified by volcanic features on the Moon compared to those on the ESRP.

Relatively fresh exposures in ESRP lava fields (Fig. 4) represent three of the four types of basaltic fissure vents on Earth (Table 1). The first two types are the progenitors of plains volcanism, typified by the ESRP (Greeley and Schultz, 1977; Greeley, 1982) as a major contributor to the landscapes of terrestrial planets. Type 3, represented by COM lava field on the Great Rift, is a chemically evolved system with multiple

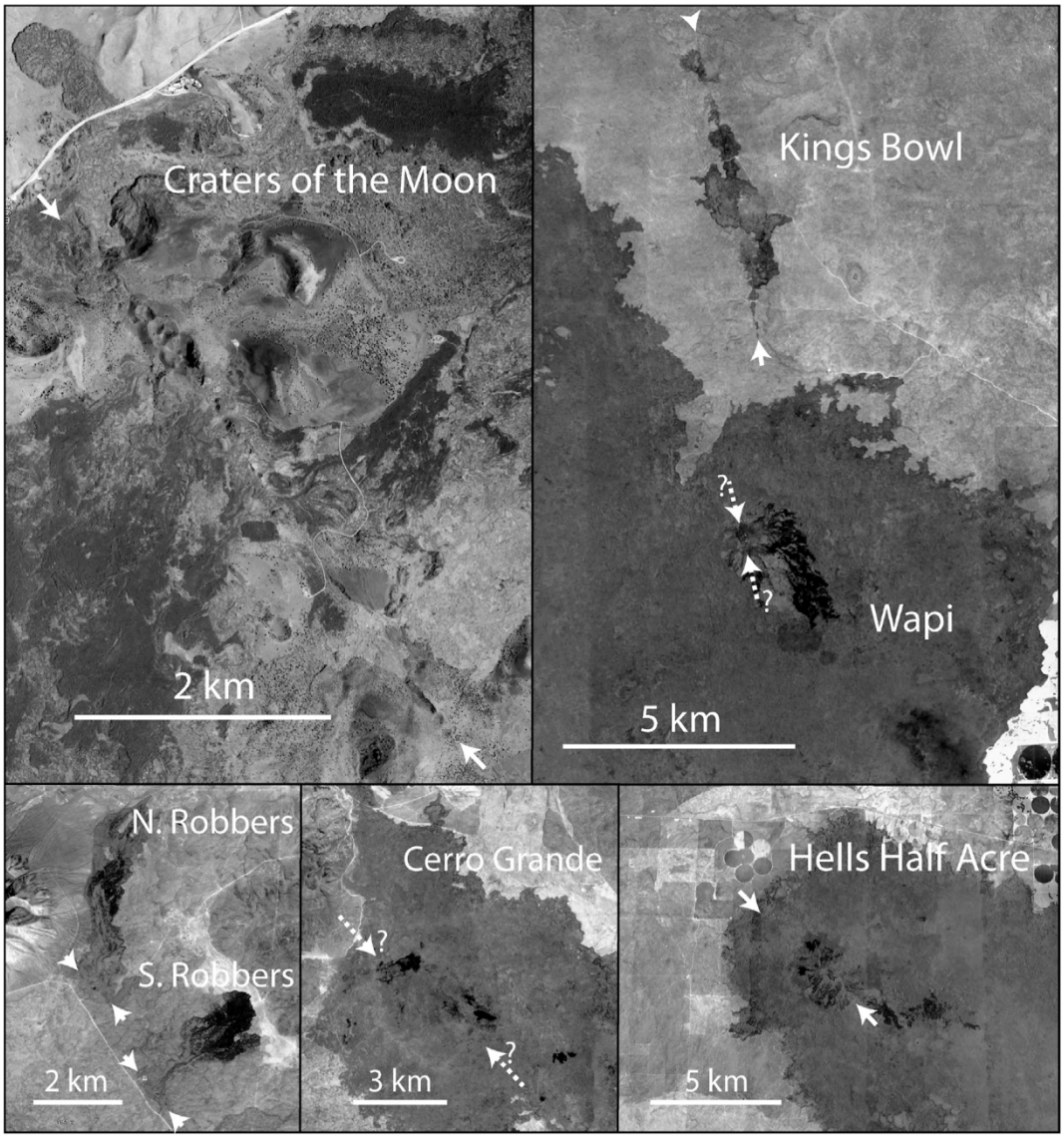

Fig. 4. Details of regions depicted in Fig. 1 (grayscale of Google Earth Landsat imagery) on the eastern Snake River Plain (ESRP). Arrows indicate interpreted ends of known fissure systems, with question marks where inferred fissure is obscured. Kings Bowl, North Robbers and South Robbers fissures are examples of type 1; Wapi, Cerro Grande and Hells Half Acre lava fields are examples of type 2; Craters of the Moon (northern segment of The Great Rift) is an example of type 3.

compositional variants (Kuntz et al., 1992, 2007; Hughes et al., 1999). Though all three types may occur in many different tectonic settings, and some are associated globally with the construction of large shields and some tectonic rift zones, the ESRP examples occur within a relatively small region. A fourth type of fissure system (Table 1) is generally a combination of multiple type 1, 2 or 3 vents. They exist elsewhere on Earth, but mainly in major oceanic and continental rift zones, and serve as an analog to large-scale high volume basalt lava terrains.

Type 1 fissures, active during short-lived eruptions or near-surface dike injections depict either the earliest stage of pyroclastic cone or low shield growth, or a temporary offshoot of a more complex system. At least one (eruptive or non-eruptive) fissure segment or series of subparallel, en echelon or complex arrangement of intersecting fissures is obvious. This type, the most basic in our scheme, is represented by Kings Bowl as the primary analog (Fig. 2), along with North Robbers and South Robbers on the ESRP (Fig. 4). Key morphological features include spatter ramparts, impounded lava flows, outflow lobes, small pyroclastic cones, phreatic explosion or collapse pits, extension cracks (or grabens), dikes, and deposits of ejected non-juvenile blocks and ash. Many surface features preserved and studied at the 7 km-long fissure system at Kings Bowl lend rationale as a primary analog for type 1 fissures (e.g., Greeley et al., 1977; Kuntz et al., 1992, 2002; Hughes et al., 1999, 2018).

Type 2 fissures are represented as monogenetic low shields or pyroclastic cones that obscure the fissure vent to the point that an actual linear feature may be difficult to locate, but a crude alignment or elongation of the structure is sometimes noticeable. Visible structures may include distal segments of the fissure system or extension cracks and grabens exposed outside the margins of the topographic cone. An elongate summit crater, or series of aligned craters representing fissure orientation may be present, which is common for low shields on the ESRP (Greeley and Schultz, 1977; Kuntz et al., 1992; Hughes et al., 1999). Analogs on the ESRP include Wapi lava field as primary, along with Cerro Grande and Hells Half Acre lava fields (Fig. 4), and many other low shields on the ESRP. Each one exhibits nested, often elongate or aligned central collapse craters at their summit, plus small lava lakes and surrounding lava flows that now obscure the original eruptive fissure vents.

Type 3 fissures are localized polygenetic eruptive fissures or spatially restricted volcanic rift zones contained in much larger volcanic provinces. Eruptions from separate vents are intermittent, over an extended time period ranging hundreds to thousands of years. These systems

typically comprise types 1 and 2 subparallel fissure vents along a linear geographic trend. Dominant structures include nested vents, cones, eruptive and non-eruptive fissures, and coalesced lava flows, often with chemically variable or evolved compositions that result in various flow morphologies and spectral signatures. Type 3 systems are represented by the COM volcanic field on The Great Rift (Fig. 4), as well as the entire East Rift Zone and Southwest Rift Zone on the flanks of Kīlauea volcano, a large polygenetic shield on Hawai'i. Additional examples of type 3 fissures (Table 1) include Ljóosufjöll in Iceland, Alu-Dalaffilla in Ethiopia, and Ardoukoba in Djibouti (Global Volcanism Project, 2013; Needham et al., 1976). Each of these polygenetic systems appears to be a distinct rift zone with multiple eruptions occurring over an extended geologic time frame. Volcanic activity at COM, for example, spans ~15 ka – 2 ka, with hiatuses up to 3000 years and chemical compositions ranging from hawaiite to latite (Kuntz et al., 1992, 2007). Surficial complexities in lava flow types, aligned cones, and even offset cones that likely cover earlier fissures, are exemplified in the northern segment of the Great Rift.

Type 4 fissures are represented by numerous basaltic feeder dikes and vents broadly dispersed throughout large igneous provinces (e.g., Columbia River and Karoo basalts). These widespread systems are characterized by dike swarms and multiple sets of aligned fissures, which may become obscured by voluminous lava outpourings. Although not found on the ESRP, they are represented in major volcanic rift zones attributed to upwelling mantle plumes, such as the Icelandic Oceanic Rift Zone (ORZ), the East Africa Rift (EAR), and continental flood basalts (e.g., White and McKenzie, 1989; Head and Coffin, 1997; Mège et al., 2004). Examples of type 4 fissure systems (Table 1) include Reykjanes Peninsula (e.g., Jenness and Clifton, 2009; Sæmundsson et al., 2018) and Laki (Thordarson and Self, 1993) in Iceland, and Manda-Inakir in Ethiopia (Barberi and Varet, 1977; Audin et al., 1990).

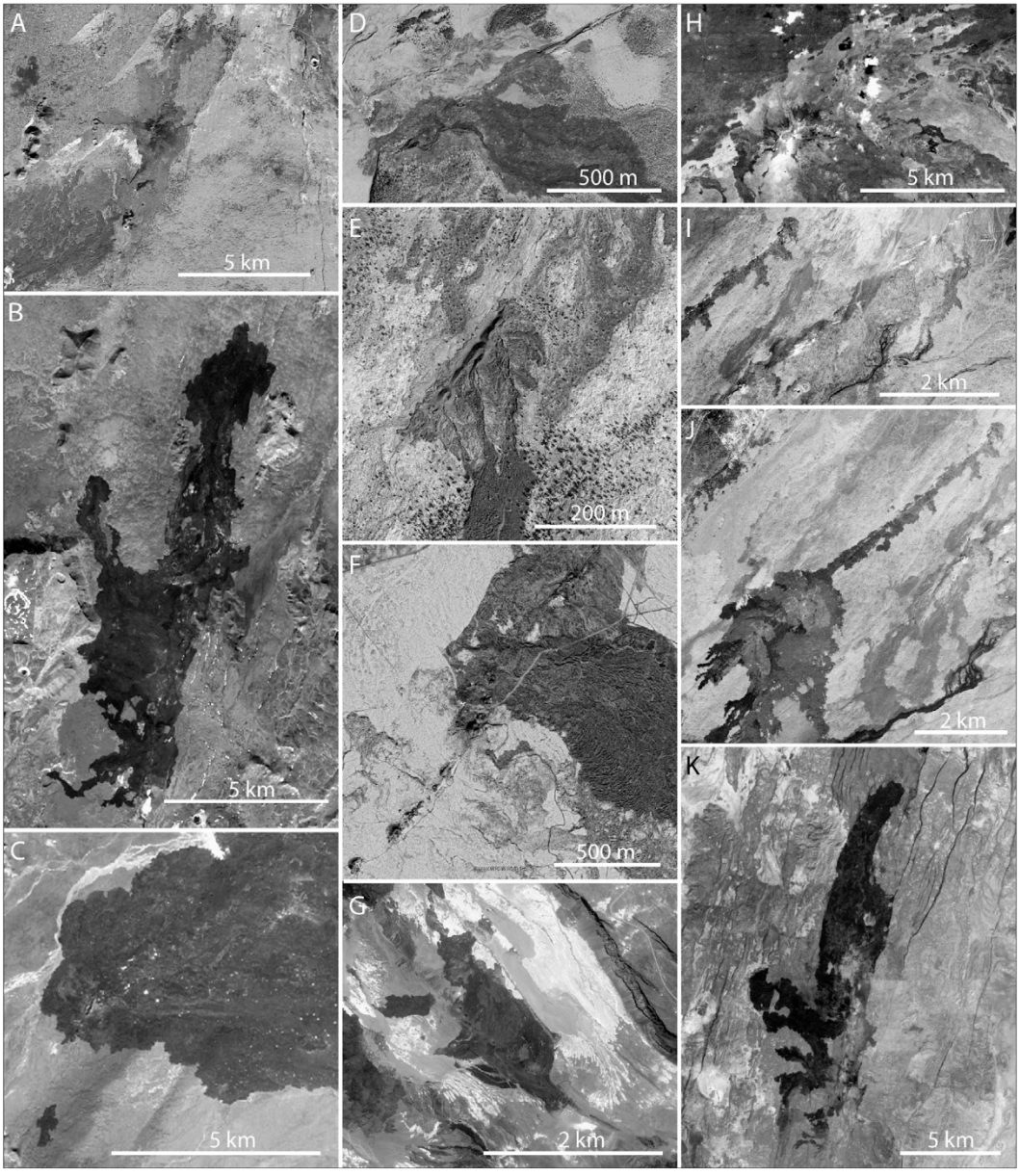

Fig. 5. Examples of basaltic fissure systems on Earth shown in grayscale of Google Earth (Landsat) imagery. Letter designations are: A = Nýjahraun (type 1), B = Krafla, C = Holuhraun, D = Kamoamoa, E = Red Cones South, F = Reykjanes, G = Ardoukoba, H = Puʻu ʻŌʻō, I = Kaʻū Desert 1974, J = Mauna Iki, K = Hertali. Each system involves at least one type 1 fissure vent; however, Puʻu ʻŌʻō (H) eruption produced a type 2 cone, Ardoukoba (G) is a type 3 (or possibly 4) volcanic rift zone, and Reykjanes (F) illustrates a series of type 1 vents along a much more extensive type 4 system. See Table 1 for precise locations.

2.3. Diversity in geologic setting

Each type of fissure may be related to more than one geologic setting. Types 1 and 2 monogenetic fissures on the ESRP, for example, comprise ubiquitous olivine tholeiites (Kuntz et al., 1992; Hughes et al., 1999, 2002). Although the ESRP examples typify plains volcanism, both types of fissure vents occurring elsewhere on Earth reveal significant variability in geologic setting and surface features (Fig. 5). Variants in morphology, volcanic features and structural components are depicted in sketch maps (Fig. 6) interpreted from the examples shown in Fig. 5. Examples of type 1 fissures within major volcanic rift zones include Nýjahraun, Krafla, and Holuhraun in Iceland (Figs. 5 and 6 A, B, and C, respectively) and Hertali in Ethiopia (Figs. 5 and 6 K). Examples of both types 1 and 2 fissure vents are also found in the summit (intra-caldera or circumferential) regions or on flank rift zones of Kīlauea and Mauna Loa on the Big Island of Hawai'i (e.g., Wolfe and Morris, 1996; Tilling et al., 2010; Lockwood et al., 1993; Neal and Lockwood, 2003), which are well-known for historic fissure eruptions.

Compared to the ESRP, the historic or recent pre-historic eruptions on the Big Island of Hawai'i, USA, illustrate similar volcanic processes although their geologic settings differ. Monogenetic type 1 examples from Kīlauea's Southwest Rift Zone (SWRZ) include Red Cones South (Figs. 5 and 6 E) and a set of en echelon fissure vents and lava flows that erupted on the Ka'ū Desert, December 1974 (Figs. 5 and 6 I). The 1919–1920 eruption of Mauna Iki on the SWRZ (Figs. 5 and 6 J), a type 1 fissure that produced a fairly voluminous outpouring of lava (noted by Lockwood et al., 1999), likely would have transitioned to a type 2 system had the eruption continued for several more years. Examples on Kīlauea's East Rift Zone (ERZ) include the Kamoamoa (Figs. 5 and 6 D) type 1 fissure and Pu'u 'O'ō (Figs. 5 and 6 H), originally a type 1 fissure that transitioned into a type 2 eruption. Kamoamoa erupted in March 2011 during a hiatus in the concurrent 1983–2018 eruption of nearby Pu'u

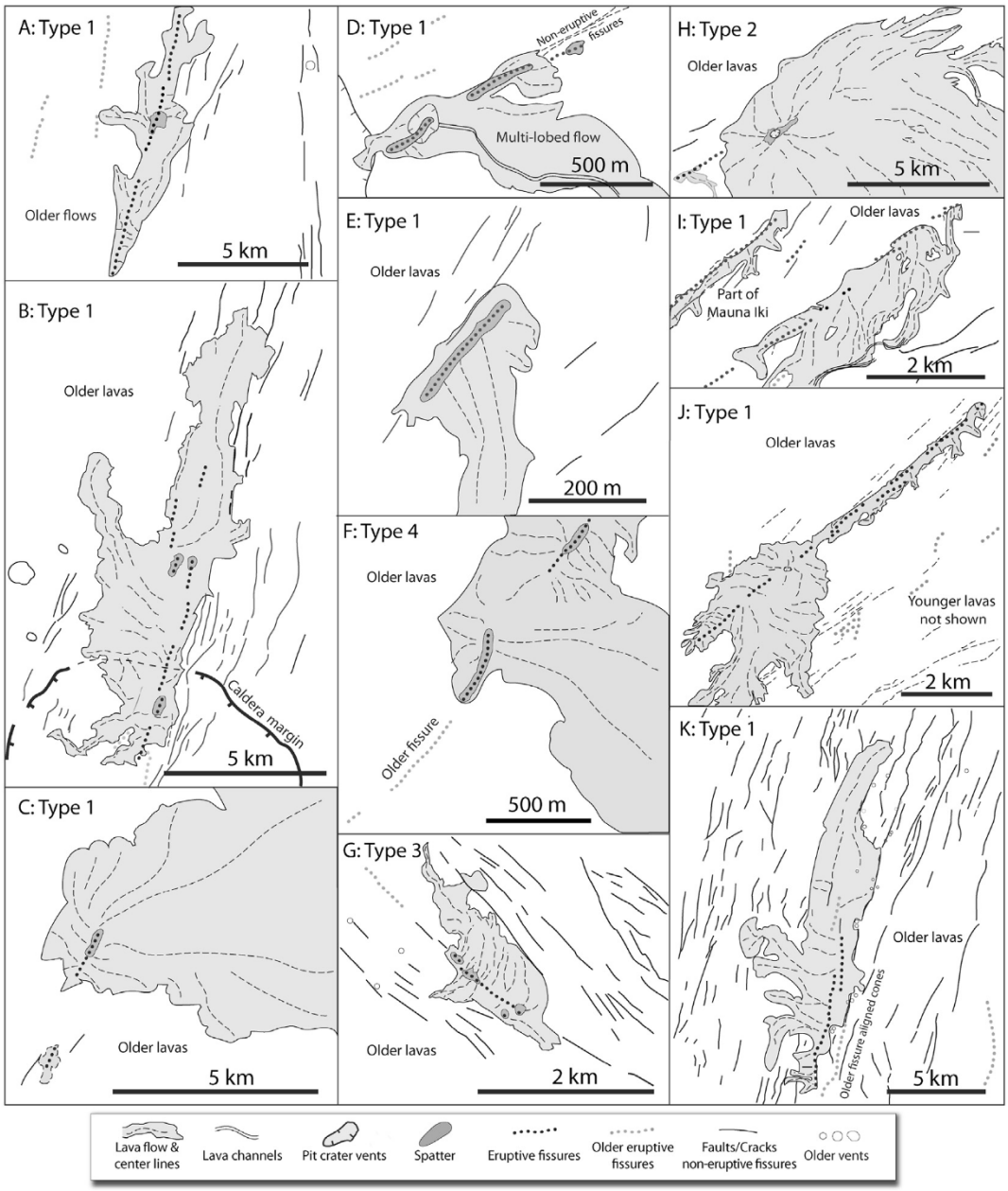

Fig. 6. Sketch maps, interpreted from Google Earth (Landsat) imagery of basaltic fissure systems shown in Fig. 5, illustrate features necessary to enable fissure categorization. Legend at bottom provides symbology for salient features mapped according to how they appear; however, some relatively small features may be misidentified due to either poor image resolution or equivocal interpretation in the absence of ground-truth field investigation.

ʻŌʻō, caused by a drop in magma level (Orr et al., 2012). Another type 2 system on the ERZ, Mauna Ulu (not shown), was active in 1969–1974 (Swanson et al., 1979; Tilling et al., 1987) with spectacular displays of lava fountaining and active lava flows in the Hawai'i Volcanoes National Park. Both Puʻu ʻŌʻō and Mauna Ulu constructed low shields on the ERZ with relatively large outflow lava fields on Kīlauea's southeast flank.

Type 3 fissures may present challenges to a strict classification. It may be argued that many type 3 fissures such as the Great Rift, ERZ and SWRZ are simply volcanic rift zones with multiple types 1 or 2 vents. This relation is borne out by the fact that these systems all contain both types of fissures (Table 1), but overall they are polygenetic with significant variability in structures and lava compositions. Likewise, type 1, and possibly types 2 and 3 fissures should be prevalent in type 4 systems; however, each smaller fissure system is typically associated with a regional cluster of fissures in the greater igneous province. As examples of such complexities, segments of Reykjanes (Figs. 5 and 6 F) or Laki fissure systems are parts of ORZ type 4 fissure systems comprising parallel chains of type 1 vents. By contrast, the type 3 Ardoukoba fissure (Figs. 5 and 6 G), which contains several type 1 vents, may be considered type 4 if the rift zone is depicted as part of the regional EAR system. In summary, types 1 and 2 fissure vents are often components of either type 3 or 4 systems, and type 3 fissures may occur within a type 4 dike swarm complex.

3. Fissure vents on the Moon

Basaltic fissure vents on the Moon are mainly recognized where dark "mantle" or "halo" pyroclastic deposits exist in mare plains and crater floors (Gaddis et al., 1985, 2000; 2003; Hawke et al., 1989). Soon after the Apollo missions, the connection between these deposits and basaltic volcanism was proposed through spectral compositions (Pieters et al., 1973, 1974) and comprehensive analyses of morphologies and geologic settings (Head, 1974; Head and Wilson, 1979). Detailed remote studies, largely via radar and spectral analyses (e.g, Gaddis et al., 1985, 2000; Hawke et al., 1989; Carter et al., 2009, 2017), interpreted the components of many localized, relatively small dark pyroclastic deposits and their association with noncircular vents formed during gas-driven explosive vulcanian eruptions. Such vents, aligned along fractures, ejected solidified non-juvenile blocks of pre-existing highland or mare wall rock as well as juvenile volcanic glass.

More recent comprehensive analysis of the generation, ascent and eruption of lunar basaltic magma by Head and Wilson (2017) reveals that explosive eruptions on the Moon produced deposits, features and structures that reflect the lower gravity and lack of atmosphere relative to their counterparts on Earth. Their assessment of volcanic features with respect to new data on (1) crustal thickness and structure and (2) the production of volatiles during magma evolution indicate a broad range in explosive eruption processes, and their respective deposits, in response to the lunar environment.

Interpretations of lunar volcanic deposits and their vent-related structures depend on visibility as either the youngest event on the surface or located where coverage due to subsequent volcanism or regolith development is minimal. Eruptive fissures on the Moon are potentially indistinct, and many can only be hypothesized from remote sensing imagery or interpreted from swales and cross-cutting fissures derived from radar data (e.g., Cahill et al., 2014). Samples of volcanic glass (e.g., Heiken et al., 1974; Delano, 1986) at Taurus-Littrow (Apollo 17) provide ground-truth evidence for pyroclastic activity, which supports the interpretation of fissures manifested as linear swales with low radar reflectivity. Remote sensing analysis at Taurus-Littrow using combined LROC NAC and Mini-RF imagery (Petro et al., 2018) reveal a compositionally distinct debris deposit and topographic ridge that likely derived from a pyroclastic fissure (Schmitt et al., 2017). Although these recent investigations indicate the likelihood of future discoveries of indistinct fissure vents (those not surrounded by dark pyroclastic deposits), we outline currently recognized structures that may enhance their exploration.

Lunar fissure vents are dominantly represented by pyroclastic blankets or cones recognized in two types of terrain, floor-fractured craters (FFCs) in highland regions or near larger impact basins, and smooth plains within or near mare basins. Gaddis et al. (2003) reviewed published descriptions of over 100 mapped lunar pyroclastic deposits and examined the compositions of 75 of them using 5-band Clementine UVVIS data. Their evaluation of locations, area, relative size, geologic setting, and compositions provides a comprehensive list of many eruptive fissures that can be examined further for morphological and volcanic interpretation. Subsequent surveys by Gustafson et al. (2012) using LROC WAC mosaic and NAC high-resolution imagery dramatically added to the number of recognized lunar pyroclastic deposits. Dark mantle deposits in Alphonsus crater, analyzed in detail using Kaguya and LROC imagery (Shkuratov et al., 2018), indicate that the low albedo relative to the surrounding crater floor is likely due to either higher FeO content or greater abundance of large basaltic clasts and glass beads. Indeed, LROC imagery has gained much importance to the on-going discovery of unusual volcanic features, such as those in Gassendi FFC (Hawke et al., 2015). These contributions indicate a growing list of documented volcanic structures (including many with exposed fissure vents) and the utility of using LROC imagery and QuickMap embedded datasets to locate and characterize them in terms of composition and morphology.

Examples of lunar fissure vents (Table 2) include known or purported volcanic structures associated with either FFCs or mare and mare-like terrains. Examples rely heavily on the interpretation of volcanism in FFCs, previously described in detail (Schultz, 1976; Jozwiak et al., 2012, 2015; Shkuratov et al., 2018) and detailed models of sill and dike evolution (Wilson and Head, 2018a, b). Previous analysis and descriptions of mare and mare-like (cryptomare) terrains (e.g. Head and Wilson, 1993; Jolliff et al., 2000; Shearer et al., 2006; Wilson et al., 2011) were used to examine possible examples of lunar mare basalt vents. The compilation of lunar vents is thus derived from previously recognized lunar pyroclastic deposits (Gaddis et al., 2003; Gustafson et al., 2012), with a few added during our QuickMap search (and careful avoidance of "dark halo craters" that may appear to be pyroclastic in origin) for additional vent structures. Locations and place names, while based on these previous works, were refined to precisely locate and designate each vent, as well as to aid in morphological description. Only vents with a topographic structure (cone, pit or crater) or a visible eruptive fissure system (fracture or linear/arcuate rille) are included.

Topography, especially elevation changes across a fissure or slopes that may dictate lava flow direction, is also used to designate vents where multiple possibilities occur along a fissure system. Fissure vent types are broadly indicated by either F (FFC) or M (mare and mare-like) based on general geologic association followed by the numerical type designation described for analogs on Earth. The lengths of fissures are estimates derived from visible structures using QuickMap tools. Lengths are reported for segments directly associated with each vent and total lengths where segments intersect a more complex system. These dimensions provide a sense of scale and complexity of the system.

3.1. FFC fissure systems

Most fissure vents in FFC settings are type 1 simple systems and a few are considered type 2 where the vent has become obscured by a topographic cone of pyroclastic deposits. Three exceptions occur in Humboldt Crater (NE, NW, SW) where vents are obscured, but designated F1 because they are associated with fractures and lack evidence of a topographic cone. We find no evidence of types 3 or 4 in FFCs, such as multiple nested vents along a single fissure or numerous fissures depicting dike swarms, and note that most are related to relatively small or very small pyroclastic deposits (e.g., Gaddis et al., 2003). This is consistent with models and gravitational considerations that indicate FFC magmatism is related mainly to shallow magma reservoirs (Jozwiak

Table 2
Lunar FFC and mare fissure vent locations and settings.

Fissure Vents	Lat. (°)	Long. (°)	Type	Fissure (km)	Total (km)	Remarks - Geologic Setting
FFC crater floors						
Airy	−18.135	5.775	F2	0	0	cone in small (35 km dia.) FFC
Alphonsus 11	−13.709	−4.194	F1	12	12	fissure partially obscured
Alphonsus 6	−13.514	−1.457	F1	3	3	Soraya vent on same fissure
Alphonsus C	−13.777	−3.382	F1	18	18	fissure partially obscured
Alphonsus Ravi	−12.511	−1.960	F1	19	30	compound fracture, NE margin
Alphonsus Soraya	−12.865	−1.622	F1	10	31	vent 6 on same fissure
Alphonsus R	−14.394	−1.915	F1	23	23	compound fracture system, indistinct
Alphonsus CA	−13.569	−4.077	F2	0	0	vent near A. 11; C fissure extension?
Gauss B	36.360	81.424	F1	70	70	FFC vent within secondary impact
Hell	−32.451	−7.691	F2	0	0	cone in small (30 km dia.) FFC
Humboldt NE	−25.691	83.225	F1	0	?	fissure obscured
Humboldt NW	−25.281	79.080	F1	0	?	fissure obscured
Humboldt SW	−28.656	79.044	F1	0	110	most of fissure obscured
Humboldt W	−26.772	78.163	F1	0	80	most of fissure obscured
Jules Verne - 1	−33.853	146.386	F1	22	48	vent along N crater margin, pos. caldera
Jules Verne - 2	−33.720	146.430	F1	6	15	smaller vent along N margin
Messala N1	40.444	59.618	F1	3	29	indistinct fissure, partially obscured
Messala N2	40.208	59.467	F1	3	29	indistinct fissure, partially obscured
Komarov	25.572	151.616	F1	13	20+	irregular, compound fracture system
Oppenheimer N	−33.572	−165.466	F1	24	~42	rel. small vent, distinct fissure
Oppenheimer S	−37.572	−166.774	F1	9	60	rel. wide vent, pos. caldera
Oppenheimer SE	−37.126	−164.600	F1	38	~55	fissure obscured by Opp. H impact
Oppenheimer SW	−36.715	−168.195	F1	12	61	rel. wide vent, pos. caldera
Oppenheimer U (NW)	−34.443	−168.204	F1	~25	?	smaller FFC within main FFC
Petavius (N)	−23.894	61.431	F1	17	81	vent & outflow channel in FFC
Petavius (SE)	−26.779	60.896	F2	0	?	fissure completely obscured
Schrodinger G	−75.280	139.173	F1	30	92	fissure partially obscured
Taruntius	5.985	46.211	F2	?	?	central cone obscures fissure
Mare Terrains						
Birt E	−20.738	−9.656	M1	12	28	vent on Rima Birt near E margin Mare Nubium
Cavalerius 1	7.498	−67.961	M1	88	?	SW margin of Oc. Procellarum
Cavalerius 2	7.591	−67.263	M1	77	?	SW margin of Oc. Procellarum
Fra Mauro	−7.183	−16.855	M1	52	156+	offshoot of Rima Parry
Frigoris E	50.303	34.379	M1	18	18	E/SE margin of Mare Frigoris
Rimae Hevelius V1	0.679	−64.998	M1	15	70	SW margin of Oc. Procellarum
Rimae Hevelius V2	−0.786	−65.337	M1	26	?	SW margin of Oc. Procellarum
Lacus Veris N	−17.772	−85.252	M1-2	4	?	ENE margin of Mare Orientale
Lacus Veris S	−18.005	−85.279	M1-2	6	12	ENE margin of Mare Orientale
Lubbock H	−3.069	42.298	M1	76	76	near rille scarp, W margin of M. Fecunditatis
Putredinis SE	25.887	1.838	M1	7	160+	Pos. dike or scarp on Rima Bradley
Rima Bradley NE	25.666	1.591	M2	0	160+	cone covers Rima Bradley
Michael	25.051	0.195	M1	3.4	55	near Rima Vladimir, fissure joins R. Bradley
Ann	25.101	−0.054	M1	4.5	55	vent near Rima Vladimir
Kathleen	25.348	−0.831	M1	7	55	vent near Rima Vladimir
R. Hyginus Crater	7.741	6.330	M1	50	230	pos. caldera, rille parallels Rima Ariadaeus
Rima Hyginus E (2)	7.675	6.567	M1	50	230	vent or pit on R. Hyginus
Rima Hyginus NW (4)	8.301	5.741	M1	102	230	vent or pit on R. Hyginus
Schluter A	−10.934	−84.217	M1	6	?	vent for Lacus Autumni (?)
Rima Reiko	18.798	27.560	M3	28	40	polygenetic (?) fissure system
Isis	18.951	27.474	M1	28	40	vent & outflow channel, Rima Reiko
Osiris	18.644	27.644	M1	28	40	vent along Rima Reiko
Rimae Maclear	12.327	20.385	M4	140	~140	multiple vents, NW margin M. Tranquillitatis
Rimae Secchi	1.132	44.211	M4	19	47	compound, NW margin M. Fecunditatis
Rimae Sosigenes A	9.224	18.724	M4	220	~220	multiple vents, W margin M. Tranquillitatis
Rimae Sosigenes C	8.329	19.084	M4	17	17	fissure crosses 87 km rille, M. Tranquillitatis

et al., 2012, 2015, 2017) derived by sill, laccolith or bysmalith intrusion when ascending dikes spread out laterally (Wilson and Head, 2018a). Only two vents that we consider to be type 2, Airy and Hell, are on cones that dominate the interiors of their host craters. Examples of FFC fissure vents (Fig. 7), selected to illustrate the variability in size (note scales) and complexity, are depicted by various fracture-vent patterns in Alphonsus, Humboldt, Oppenheimer and Schrödinger craters. Vents are invariably associated with fractures that exhibit irregular polygonal, radial or concentric patterns (Jozwiak et al., 2012) with few linear segments. Many fractures intersect others in complex arrangements, with or without fissure vents, which is likely a manifestation of various subsurface reservoir sizes and shapes, and also the likelihood that some dikes fail to erupt because they intrude the network of magma reservoirs instead (Wilson and Head, 2018a).

Fracture and volcanic vent patterns in FFCs, as well as topographic structures, are thus generally inconsistent, and provide evidence for complexities and variabilities in magmatic systems (Jozwiak et al., 2015, 2017). Several examples illustrate the differences in fracture patterns among well-documented FFC systems. Circumferential fractures in Alphonsus, a crater with multiple vents, are less well-defined and more obscured than those in Humboldt, which has fewer vents. Fracture patterns in Oppenheimer are more like those in Alphonsus, yet their respective vents (except Oppenheimer N) have distinct morphological differences. Schrödinger crater has well-defined radial fractures, but the single noticeable vent in the crater (G) lies on a segment that does not appear to have a radial orientation.

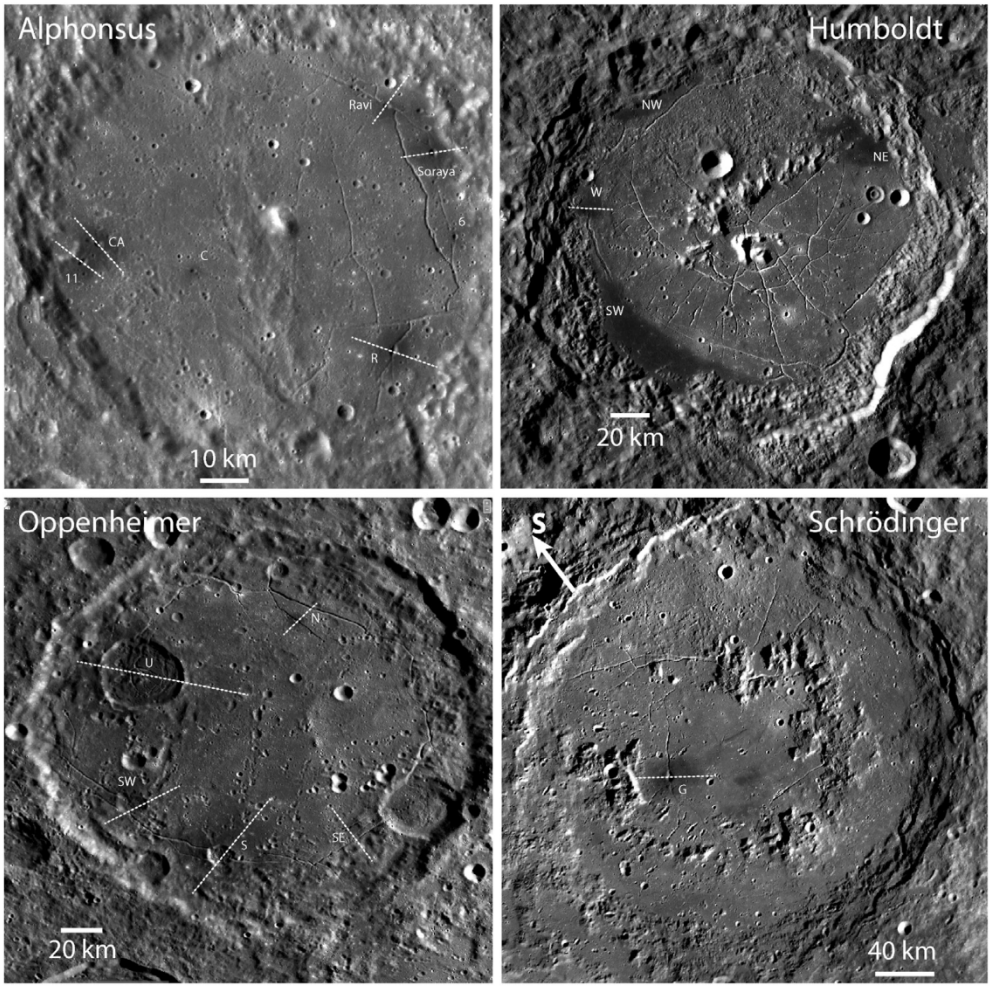

Fig. 7. Examples of fissure vents in floor-fractured craters (LROC WAC imagery) representing distinctly different crater sizes, fracture patterns, and spatial arrangements of vents (see detailed maps and analyses in Jozwiak et al., 2012, 2015, 2017; and Wilson and Head, 2018a). Dark pyroclastic deposits, clearly visible and predominantly along fractures, fundamentally indicate associations with volcanic vents. Dashed white lines depict topographic profiles (Fig. 10) derived from QuickMap tools. See Table 2 for exact vent locations.

3.2. *Mare fissure systems*

Fissure vents associated with lunar mare and mare-like plains mostly exhibit type 1 morphologies that lie on distinctly linear rilles (Table 2, Fig. 8). Several vent systems are tentatively designated type 4; however, that association is unclear as many mare vents as well as rille segments have been obscured by subsequent volcanic activity. Evidence of this is fairly common, such as the vents on Rima Bradley, which are surrounded by dark pyroclastic deposits, and a row of cones and pyroclastic deposits along the western rille of Rimae Parry graben (see Head and Wilson, 2017). Both of these examples indicate that lunar volcanic deposits can partially or even completely obscure segments of an eruptive fissure.

Some type 1 mare basalt vents actually lie on complex rille networks (rimae) where multiple vents are likely to be discovered. This leads to the suggestion that many mare basalt vents, like flood basalt fissure systems on Earth, should be considered type 4. Mare vents, like FFC vents, exhibit some variation in their related rille systems, and most are associated with extensive fissure systems with total lengths of tens to hundreds of kilometers (Table 2). A global search and mapping effort using Kaguya 7 m/px and LROC NAC data is warranted as additional mare vents may be discovered, especially along the ubiquitous rilles associated with mare basins.

Morphological variations among linear rilles and vents (Table 2, Fig. 8), like FFC systems, reflect complex processes in mare basalt volcanism. One pertinent observation is that Rima Bradley, at least 160 km long, extends through both mare and non-mare terrains along a system of subparallel rilles and cross-cutting smaller rilles SE of Mare Imbrium. The rille appears to be completely covered in some areas by pyroclastic deposits, and either exposed or partially covered in other segments. Small well-exposed vents nearby, Kathleen, Ann and Michael (Fig. 8) possibly contributed to Rima Bradley being partially covered by pyroclastic deposits. Another unique feature, located along Rima Hyginus, is a coalesced series of dike-induced collapse pit craters (e.g., Wilson et al., 2011). Rima Hyginus, which is not directly within a mare basalt terrain (it lies south of Mare Vaporum and west of Mare Tranquillitatis), is complicated further by (1) a sharp difference in the alignments of the eastern and northwestern segments, and (2) an apparent offshoot extension of Rima Hyginus west of the intersection that aligns with the eastern segment. The largest vent, Hyginus crater, is likely a collapse pit crater or even a caldera (Wilson et al., 2011), that developed close to that intersection. High-resolution imagery of the crater floor also illustrates the presence of irregular mare patch (IMP) surfaces similar to inflated lava flows (e.g. Garry et al., 2012; Braden et al., 2014).

A compelling example of "mare-like" volcanism is represented by fissure vents in Lacus Veris (Fig. 9), located in the ENE sector of Montes Cordillera, a multi-ring impact basin that contains Mare Orientale. The region is one of the very large pyroclastic deposits noted by Gaddis et al. (2003), which suggests that these features probably have been covered by a thin layer of pyroclastic material. Vents are apparently conical structures (either pyroclastic cones or low shields) with clear association to irregular fissures, but there is no obvious relation to mare volcanism other than the proximity to Mare Orientale. More importantly, this system may represent a rarely preserved transition from type 1 to 2 fissure eruption, with implications for incipient magmatism not observed in much larger mare terrains.

Other examples of mare fissure vents appear to have less complicated

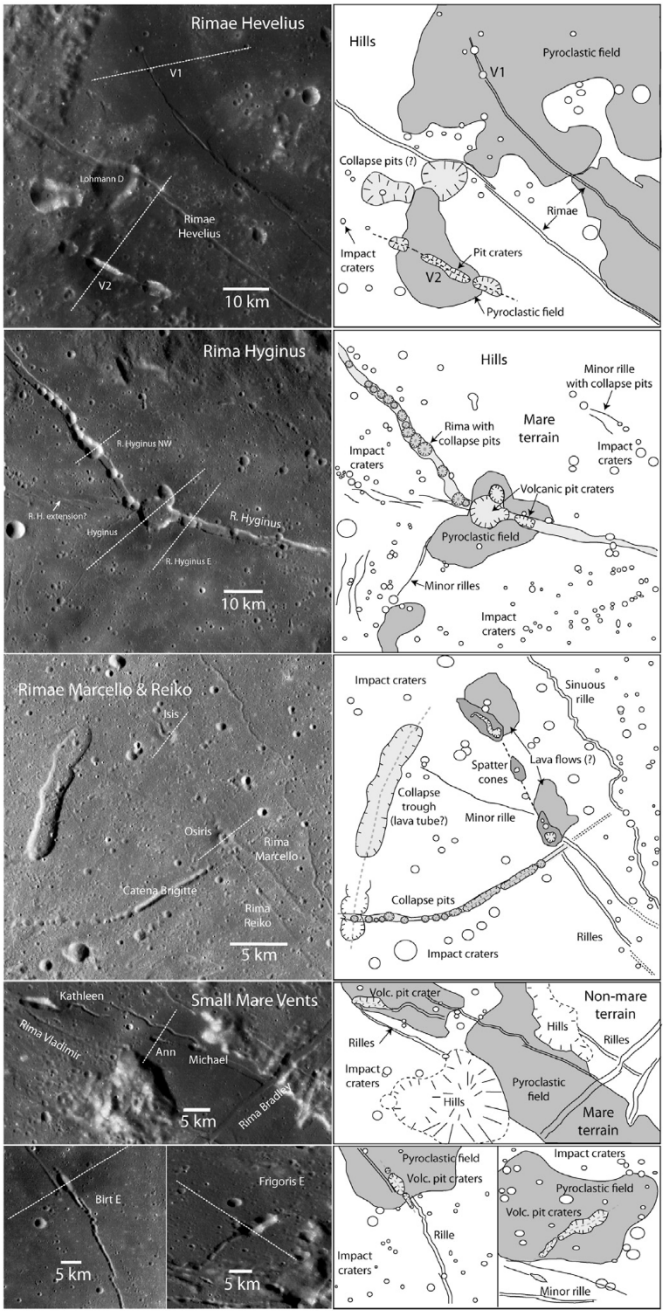

Fig. 8. Selected lunar fissure vents in mare and mare-like terrains (LROC WAC mozaics, left panels) illustrating variability in vent/rille associations and morphologies for Rimae Hevelius, Rima Hyginus, Rimae Marcello/Reiko (Kaguya TC image), and other small mare vents. Dashed white lines depict topographic profiles (Fig. 11)(derived from QuickMap tools. Sketch maps (right panels) illustrate selected features observed in LROC images that can be used to evaluate geologic processes. See Table 2 for exact vent locations.

associations with rilles. Isis and Osiris, both of which lie on Rima Reiko (Fig. 8), individually display simple type 1 characteristics (spatter cones most likely) typical of plains volcanism (e.g. Greeley, 1982). However, they occur as multiple, possibly polygenetic eruptions along with others on a relatively complex rille. Thus, Rima Reiko is considered to be a type 3 polygenetic fissure system (Table 2) although relative ages and compositional variability cannot be determined. Likewise, the two vents in the Rimae Hevelius region (V1 & V2) exhibit type 1 morphology, but the system of vents among multiple rilles indicates a potential type 4 system. Each of these vents, with fairly large pyroclastic deposits, suggests higher eruption explosivity (and volume?) than Isis or Osiris. These observations indicate that perhaps many type 1 mare vents in rimae settings, now buried by younger flows, would represent either complex type 3 fissures or type 4 regions with multiple fissures.

3.3. Lunar fissure profiles

Fissure vent morphologies on the Moon (Figs. 7–9) depict the differences in volcanic processes and geologic settings between FFC and mare basalt eruptions. Morphological variances between eruptive vents (and collapse pits) are examined further in topographic profiles of FFC (Fig. 10) and mare-like (Fig. 11) fissure vents, constructed using High-resolution Lunar Topogaphy (Barker et al., 2015) SLDEM 2015 & LOLA data (3–4 m vertical accuracy) in QuickMap tools. Profile directions run from the westernmost point to the easternmost point along each line depicted in Figs. 6–8. The extent of pyroclastic halos around many FFC vents (Fig. 7) also enables the apparent cross section of topographic cones in some profiles.

Profiles of FFC vents (Fig. 10) demonstrate that, regardless of scale, most exhibit a typical "V" shape with topographically higher flanks relative to surrounding crater floor surfaces. By contrast, non-eruptive segments of fractures (FFC rilles) exhibit "V" shape profiles without raised rims such as the rille in Alphonsus Soraya profile (Fig. 10 upper). Although only one profile direction is illustrated, each one reveals a topographic cone or rampart built up by the surrounding pyroclastic deposits. Compared to COM pyroclastic (cinder) cones as analogs (Fig. 10, inset) lunar FFC vent constructs are larger and have much deeper crater floors extending to depths (>200 m in many; Shrödinger G is > 300 m deep) well below the surrounding terrain. This morphological difference is most likely related to FFC vents being derived by vulcanian eruptions of non-juvenile material (e.g., Head and Wilson, 1979; Jozwiak et al., 2015) compared to the strombolian style of COM eruptions.

Exceptions to the "V" shape of FFC vents include Humboldt W and Oppenheimer U, SW and S, all having irregular floors, relatively large diameters, and overall morphology that is inconsistent with a simple fissure vent process. Regardless of pyroclastic material exposed in the surrounding regions, some of these craters such as Oppenheimer U are likely due to impacts subsequent to main crater formation. Indeed, Oppenheimer U apparently has floor fractures and raised rim, and appears to be a small FFC impact within the larger FFC. By contrast, Oppenheimer S and SW exhibit pyroclastic halos, which reveal volcanism possibly related to the formation of relatively large collapse pit craters or even calderas.

Topographic profiles across mare fissure vents (Fig. 11) confirm the aforementioned variability in overall vent constructs along linear rilles shown in Figs. 7 and 8. The most prominent, represented in the profiles of Ann, Birt E and Frigoris E, and Rimae Hevelius vents V1 and V2, are variable in size with "V" shapes and pyroclastic halos on apparently raised topographic rims. Similar to FFC vents, with vent floors well below the surrounding terrain, these are considered to be regular type 1 fissures under the proposed classification and represent the dominant morphology of fissure vents in mare terrains (Table 2). Similar to most FFC vents, they also likely represent deposits of non-juvenile basalt clasts derived from a vulcanian explosive eruption that disrupted and ejected a solid carapace of cooled magma at the top of the dike (e.g., Head and Wilson, 2017).

Other mare vent morphologies, while less represented on the lunar surface, are structurally similar to their plains-style analogs on the ESRP although the lower lunar gravity would likely result in lower-profile constructs (e.g., Head and Wilson, 2017). Osiris and Isis, the two type 1 vents similar to the Kings Bowl fissure, have profiles that appear overall similar to Cottrells Blowout (low shield) and COM pyroclastic cones (Fig. 11) on the ESRP. Likewise, the profiles of transitional type 1–2 fissure vents in Lacus Veris, N and S, have striking similarity to the Wapi low shield. Although the eruptive fissure for the S vent is well-exposed, the fissure for the N vent is not as prevalent, which suggests that these

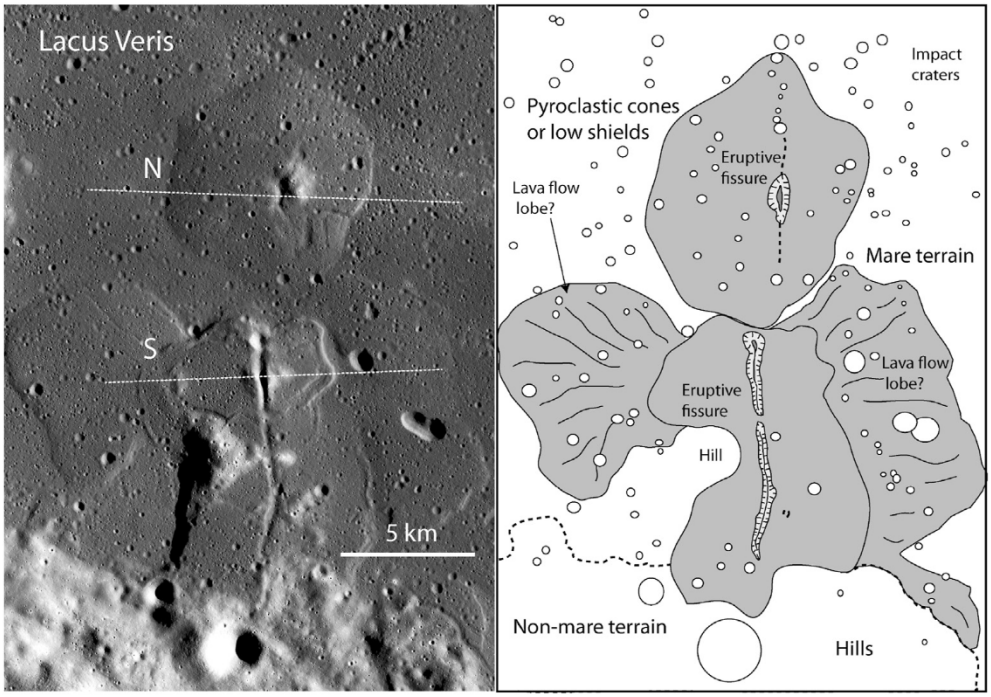

Fig. 9. Two unique vents in Lacus Veris (Kaguya TC image, left; sketch map of region, right), each with a topographic cone structure along an eruptive fissure located in the ENE sector of Montes Cordillera (east of Mare Orientale). Note that the fissure is nearly obscured by deposits from the northern (N) cone and that a third vent is likely south of the southern (S) cone. The region is also covered by a thin veneer of pyroclastic material (Gaddis et al., 2003). Dashed white lines depict topographic profiles (Fig. 11) derived from QuickMap tools. See Table 2 for exact vent locations.

two lunar vents represent a possible shield-building episode of volcanism in Montes Cordillera.

Profiles of features along Rima Hyginus (Fig. 11) represent possibly complex volcanic scenarios. Although the profile of R. Hyginus E reveals the typical "V" shape like other volcanic vents, R. Hyginus NW and the namesake Hyginus Crater are flat-floored. The likelihood that these features and others along the rille are collapse pit craters associated with arrested dike intrusion (Wilson et al., 2011), the "V" shape of R. Hyginus E cannot be used as singular evidence of volcanic activity. Moreover, many of the large pit craters along Rima Hyginus have much larger widths relative to depths compared to other vents in Fig. 10. The largest one (Hyginus Crater) may actually be a caldera similar to those at the summits of major shield volcanoes such as Mauna Loa and Kīlauea. The floor of Hyginus also has irregular mare patch (IMP) units, which are interpreted as geologically young flows (Braden et al., 2014) that formed as either inflated lava flows (Garry et al., 2012) or by the eruption of magmatic foams (Qiao et al., 2017, 2019; Wilson and Head et al., 2002).

Physical dimensions derived from QuickMap (Table 3) for profiled (Figs. 9 and 10) and non-profiled vents and craters indicate significant variability in rim-to-rim widths, measured perpendicular to rille or fissure direction, rim-to-floor depths, and a large range in elevations. The widths and depths of FFC examples, with the exception of Oppenheimer U, S and SW, and Jules Verne – 1, as notable outliers, range 0.96–6.1 km and 45.4–1206 m, respectively (minima represented by Taruntius and maxima represented by Schrödinger G). Minimum vent elevations, i.e., crater floors, range −1675 m for Alphonsus 6 down to −5487 m for Schrödinger G, which also reflects a large difference in crater size (Fig. 7). The outliers, Oppenheimer U, S and SW, range 11.5–38 km in width and 769–1911 m in depth, with elevations from −5408 m down to −5893 m. The other FFC outlier crater, Jules Verne - 1, has a 4.7 km width, 253 m depth and bottom elevation of −2205 m. Mare-like vents listed in Table 3, with the exception of Hyginus Crater at 11.45 km width and 817 m depth, show a range in width of 0.65–6.9 km and a range in depth of 22–1060 m. Floor elevations range −462 m (Schluter) down to −3290 m (Frigoris E). These dimensions fall approximately within the range of FFC vents although both sets of dimensions range over at least one order of magnitude.

A near-linear wide range of plotted crater depths vs. widths (Fig. 12) is evident in mare and mare-like terrains, and FFC vents bear a close association to that trend. The apparent uniformity in width/depth ratio suggests a potential correlation between vent size and volume or intensity of eruption. The volume of magma necessary to have produced either an FFC or mare individual eruption is unclear; however, inferences can be made regarding volcanic style and deposits. Eruptive models for both types reveal that FFC eruptions are related to relatively small shallow sill reservoirs below the crater floor (Jozwiak et al., 2012, 2015; 2017; Wilson and Head, 2018a) and that mare fissure eruptions are most likely derived from dikes that ascend from great depths and do not involve a shallow magma reservoir (e.g., Wilson and Head, 2017). Except for Schrödinger G, this is consistent with the largest structures in Fig. 12 being represented in mare-like terrains. Also, the smallest and largest FFC vents shown in Fig. 7, Alphonsus C and Schrödinger G, occur in the smallest and largest craters, respectively.

3.4. Implications for lunar magmatism

Examples of fissure vents provide a cursory assessment of two major styles of basaltic volcanism on the Moon. Most fissures in lunar FFCs are noticeably type 1, recognized as pyroclastic deposits adjacent to fractures. The majority of type 1 fissure vents in FFCs is consistent with recent studies that attest to dike-fed eruptions from relatively small, local networks of magma reservoirs possibly fed from deeper sources (e.g., Wilson and Head, 2018a). Scarce examples exist of type 2, and neither type 3 nor 4 can be unequivocally identified in FFC terrains. Vents related to mare basalts and mare-like terrains are not so straightforward, yet the appearance of multiple type 1 vents along complex rilles and in rimae swarms suggests that type 4 fissure systems dominated the vast mare basalt eruptions. These observations strongly suggest that the visible type 1 or 4 mare fissures on the lunar surface represent only a meager fraction of mare basalt vents. The same may not be true for FFC fissure vents, especially those in the highlands.

As in Earth analogs, each type apparently reflects a unique and representative mode of volcanism with minimal variation in style; however, the few but notable variants provide important implications for magmatic evolution. However, recent modeling of lunar eruptions suggests that variants may be related to a series of events occurring in single

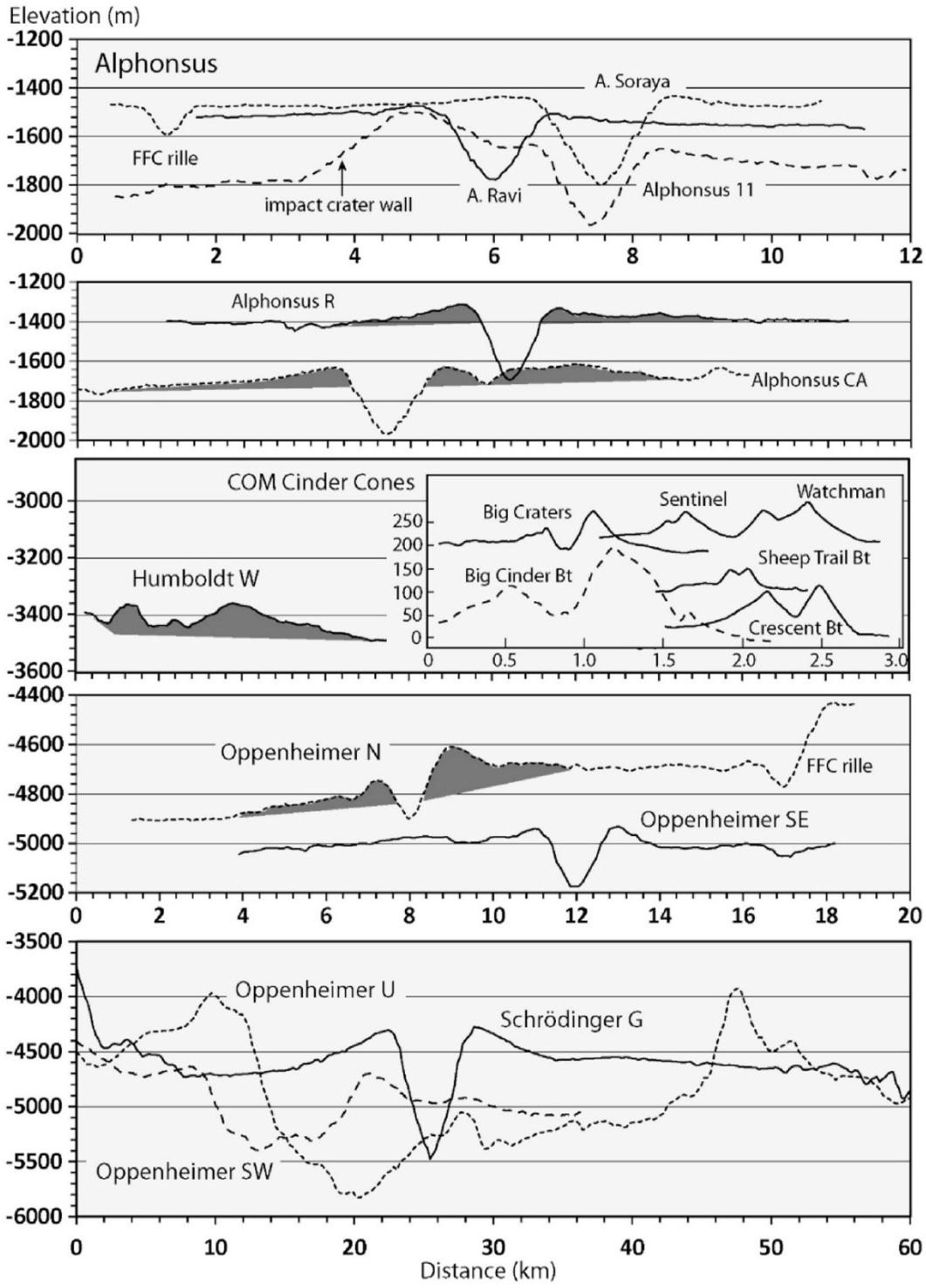

Fig. 10. Topographic profiles across FFC vents shown in Fig. 7 and pyroclastic cones from the COM system along the Great Rift (inset, vertical scale in m, horizontal scale in km). Dark shaded regions indicate the surficial extents (unknown depths) of pyroclastic deposits visible in LROC imagery. Note different distance scales between the upper, combined middle three, and lower groups.

eruptions (e.g., Wilson and Head, 2018b). Differences in fracture patterns, vent sizes and shapes depicted in FFCs may reflect significant disparities in magma composition, rheology and eruption velocities, magma source depths and volumes (e.g., Head and Wilson, 2017; Sehlke and Whittington, 2020), not to mention the likely variability in crust and impactor compositions and physical properties. Disparities in mare fissure vents, rille shapes and sizes between the few examples examined here imply the likelihood of complex magmatic processes leading to variability among lava flow and pyroclastic compositions.

Vast lava flows that cover mare and cryptomare terrains require large-volume eruptions of low-viscosity basaltic magma (e.g., Head and Wilson, 1992; Hiesinger and Head, 2006; Hiesinger et al., 2011), with high-flux, hawaiian style fire fountain lava outpourings (phase 2 of Wilson and Head, 2018b) compared to FFC eruptions. Similar to flood basalts on Earth, mare fissure vents that fed such large scale eruptions are mostly obscured. Though only a few can be observed and measured, the

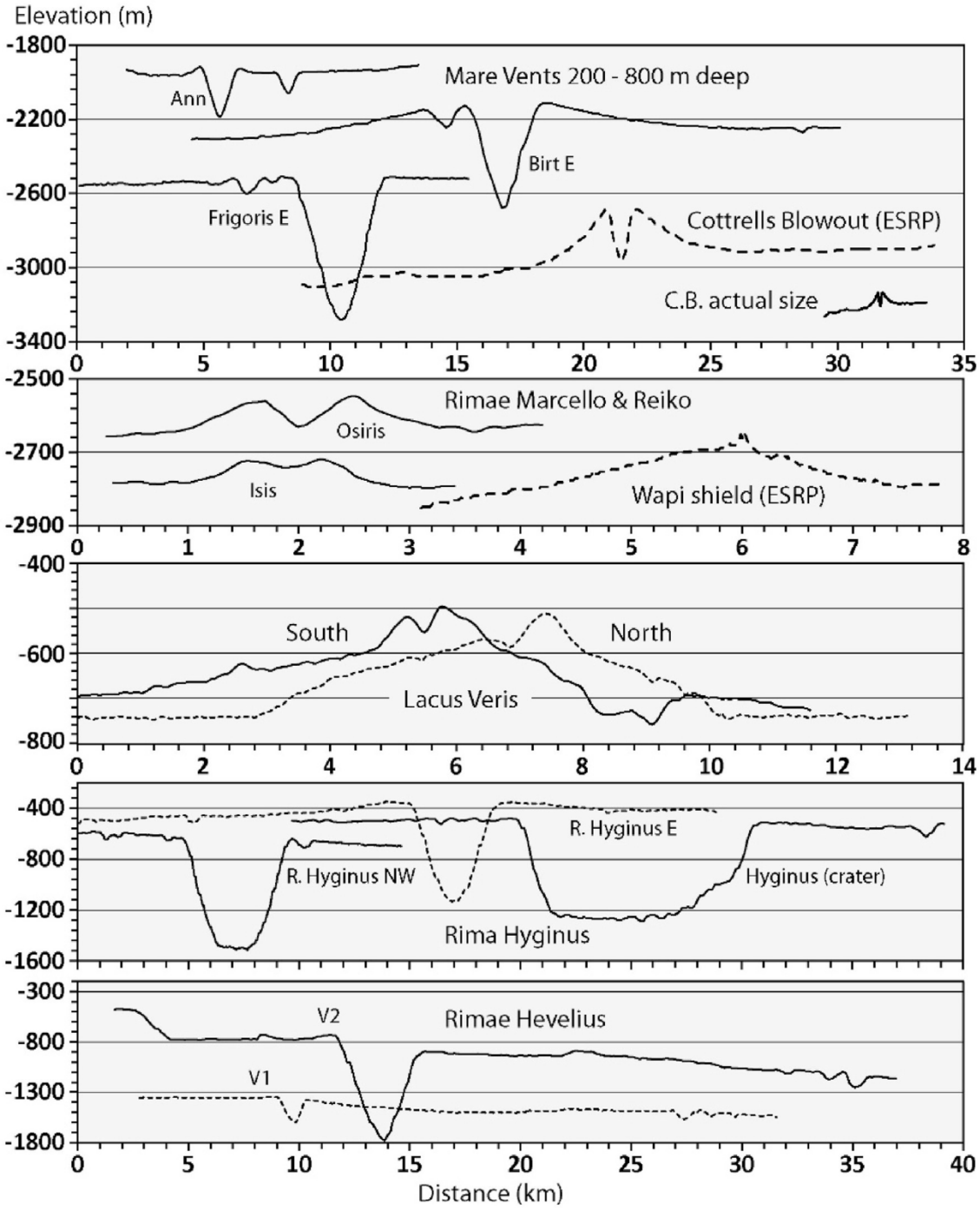

Fig. 11. Topographic profiles across mare fissure vents shown in Figs. 8 and 9.

range in dimensions likely reflects variability in explosivity or magma effusion rates. Regardless, some mare vents are morphologically similar to FFC vents.

The eruptions from relatively small FFC vents such as those in Alphonsus produced small pyroclastic cones or thin blankets of solid basaltic clasts ejected during vulcanian eruptions around vents, but not lava flow fields. Although these observations imply short-lived explosive strombolian or vulcanian style eruptions and low magma production rates, more detailed investigations of eruption dynamics reveal magmatic complexities involving shallow sills and dikes (e.g., Schultz, 1976; Jozwiak et al., 2012; Thorey and Michaut, 2014; Wilson and Head, 2018a) and correlations to magma driving pressure, effusion rates, and crustal properties including thickness and density (e.g., Jozwiak et al., 2015; Thorey et al., 2015; Head and Wilson, 2017). Regardless of such complexities and variable conditions, relatively small FFC fissure vents (Fig. 12) represent low-volume magmatism compared to mare basalts.

Given that most mare units could be classified as type 4 fissure systems, their overall depiction as components of large igneous provinces is evident, with flood basalts and major rift systems on Earth as analogs. Chemical and mineralogical variety among mare basalts attests to myriad processes related to lunar magmatism (e.g., Neal and Taylor, 1992; Snyder et al., 1992). Such variability has yet to be demonstrated in FFC volcanic deposits although complexities may be possible even in very small magmatic systems (e.g., Hughes et al., 2017, 2018).

Several postulated (outlier) vents that fall significantly off the mare vent trend in Fig. 12 possibly indicate polygenetic volcanic processes

Table 3
Lunar FFC and mare fissure vent dimensions.

Volcanic Fissure Vents	Width (km)	Min Elev. (m)	Max Elev. (m)	Depth (m)
FFC Vents				
Alphonsus 11	1.82	−1966	−1633	333
Alphonsus 6	1.97	−1676	−1447	229
Alphonsus C	1.60	−1783	−1587	197
Alphonsus CA	2.70	−1972	−1635	337
Alphonsus R	2.29	−1698	−1315	383
Alphonsus Ravi	2.00	−1778	−1474	304
Alphonsus Soraya	2.06	−1801	−1435	366
Gauss B - fissure-cone	3.57	−2955	−2390	565
Humboldt W	2.32	−3442	−3359	83
Jules Verne - 1	4.72	−2205	−1952	253
Jules Verne - 2	2.62	−2196	−1962	234
Messala 1	2.26	−2149	−1909	240
Messala 2	2.10	−2087	−1921	166
Oppenheimer N	1.74	−4899	−4607	292
Oppenheimer U (NW)	38.0	−5840	−3929	1910
Oppenheimer S	11.5	−5893	−4645	1250
Oppenheimer SE	2.01	−5178	−4936	241
Oppenheimer SW	13.0	−5408	−4640	769
Petavius (N)	2.19	−2461	−2260	200
Petavius (SE)	1.61	−2247	−2111	197
Schrödinger G	6.12	−5487	−4281	1210
Taruntius	0.96	−2377	−2331	45
Mare Vents				
Ann	1.60	−2188	−1920	268
Birt E	3.11	−2685	−2114	572
Cavalerius 1	6.91	−2018	−1202	816
Cavalerius 2	2.06	−1801	−1435	366
Frigoris E (fissure?)	4.35	−3290	−2512	777
Isis	0.65	−2747	−2725	22
Lacus Veris N	1.02	−587	−512	75
Lacus Veris S	0.55	−553	−496	57
Lubbock H	3.92	−2015	−1596	419
Osiris	0.79	−2633	−2549	84
R. Hyginus (Crater)	11.5	−1291	−475	817
Rima Hyginus E (2)	5.40	−1139	−345	794
Rima Hyginus NW (4)	5.33	−1527	−629	898
Rimae Heveliuis V1	1.53	−1615	−1356	259
Rimae Hevelius V2	4.33	−1791	−731	1060
Rimae Secchi	2.83	−1626	−1302	324
Schluter (vent & channel)	1.73	−462	−346	117

where multiple eruptions over time produced close-spaced interfering vents. The greater relative widths and relatively flat floors of these craters suggest multiple eruptions (or lava lakes) over relatively long periods of time. Such characteristics are typical of collapse pit craters on low shields like Wapi and Cerro Grande, or calderas in the summit regions of Kīlauea and Mauna Loa on Hawai'i. Actually, Oppenheimer U, a gargantuan crater by volcanic standards, is most likely an impact crater. The relative widths of Oppenheimer S and SW, Hyginus (all >10 km) and possibly Jules Verne-1 (4.72 km) may indicate the questionable existence of lunar calderas or caldera-like features in both mare and FFC terrains (e.g., Head and Wilson, 1991; Wilson et al., 2011; Spudis et al., 2013).

4. Volcanism on Mars

Volcanic landforms on Mars were confirmed when the Mariner 9 (1971) and Viking (1976) missions revealed many structures ranging from very large shields to small cones and low shields (e.g., Hodges and Moore, 1994). Viking Orbiter imagery provided the mainstay of photogrammetric data used to characterize relatively large volcanoes such as montes (major shields), tholi (minor shields and relatively small cones) and paterae (low-relief shields with summit depressions) of the Tharsis and Elysium regions. The imagery also revealed extensive networks of fossae (grabens and fractures), especially in northern Tharsis and Alba Mons regions (Fig. 2).

Much smaller low shields and other volcanoes having less than ~20 km diameters were also recognized in Viking imagery (e.g., Hodges, 1979; Moore and Hodges, 1980). These small edifices covering the Tharsis, Elysium and other plains on Mars (e.g., Syria Planum and Tempe Terra), were classified by Greeley (1977, 1982) as dominant components of basaltic plains volcanism typified by low shields having similar physical dimensions as those on the ESRP. Subsequent to the large amount of data derived from Viking Orbiter imagery, detailed analyses of smaller volcanic structures advanced rapidly with images from the Mars Orbiter Narrow-Angle Camera (MOC), Thermal Emission Imaging System (THEMIS), High Resolution Stereo Camera (HRSC), and topographic data from the Mars Orbiter Laser Altimeter (MOLA). These platforms were enhanced by the inclusion of Context Camera (CTX, Malin et al., 2007), enabling images with spatial resolution of ~5–6 m/pixel to be extracted from the Mars Image Explorer website (https://viewer.mars.asu.edu/viewer/ctx#T=0) operated by the ASU Mars Flight Facility.

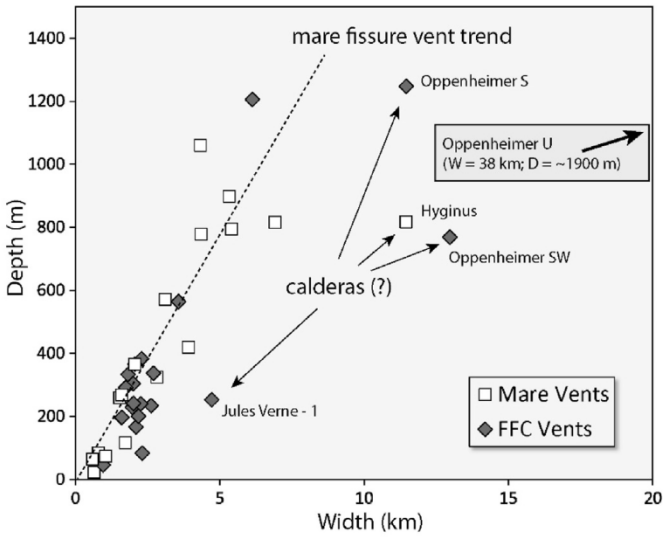

Fig. 12. Plot of depth vs. width of fissure vents on the Moon observed in mare-like (including cryptomare) and FFC settings (Table 3). The nearly linear trend in rim-to-rim widths and rim-to-floor depths likely represent similar volcanic styles with variation in eruptive volumes or explosivity. Craters that fall far off the trend include purported calderas and Oppenheimer U, which is probably an impact crater, that plots outside the field.

The analysis of low shields and related landforms in the Tharsis region (e.g., Wilson and Head, 1994; Bleacher et al., 2009; Hauber et al., 2009, 2011; Wilson et al., 2009; Richardson et al., 2017; Peters and Christiansen, 2017) provide comprehensive knowledge of their morphologies, inherent volcanic processes, geologic settings, relative ages and implications for magma genesis. These contributions further provide the background and rationale to survey similar low shields and other small landforms on Mars, especially in light of the connections to analog features on the ESRP and other regions on Earth (Greeley, 1977, 1982; Hodges, 1979; Moore and Hodges, 1980; Hodges and Moore, 1994).

Although the intent here is not to reproduce or provide additional details to these and many other previous studies, CTX imagery is used to associate representative fissure vents in the greater Tharsis region with known Earth analogs. The volcanic terrains are characterized by relatively unobscured extensive lava plains that developed during the latest Hesperian and Amazonian (AHv) periods (Tanaka et al., 2014). Yet many key features related to fissure eruptions are not evident like they are on Earth. For example, over 400 likely FFCs are identified on Mars by Bamberg et al. (2014) in a comprehensive study of processes and the relations of FFCs to geographic location and environment. Although their models present viable arguments to link FFCs to chaotic terrain, outflow channels and the global dichotomy boundary, as well as reveal several likely origins including volcanic activity, the presence of specific fissure

vents and volcanic deposits remains unclear. Another example is relevant to flood basalts on Mars. The surface morphology of flood lavas on Mars is similar to analog lava flow fields in Iceland (Búrfells, Laki and Krafla), yet the martian lavas cannot be positively correlated to their eruptive sources (Keszthelyi et al., 2004). Thus, fissure vents related to FFCs and the ubiquitous flood lavas on Mars may be difficult to identify.

4.1. Examples of martian fissure vents

Representative low shields and fissure vents were selected from numerous examples having roughly the same spatial scale as ESRP structures. We further restricted the examples to obvious volcanic systems although many non-eruptive fissures, fossae with grabens and fractures, and other features related to volcanic processes can be observed in the region. Included here are low shields that lie on the plains east and south of Pavonis Mons (Fig. 13 A, B and D), east-northeast of Arsia Mons (Fig. 13 F), and approximately midway between Olympus Mons and Alba Mons (Fig. 13 E) all considered to represent type 2 vents. The well-exposed fissure that transects another shield east-northeast of Arsia Mons (Fig. 13 C) is considered a type 1 fissure with multiple vents, a relatively scarce feature on Mars, or a transitional type 1–2 fissure. Each type 2 shield (as well as many others found in CTX images) exhibits morphological evidence of similarity to low shields on the ESRP (e.g., Greeley, 1977, 1982). Summit regions are characterized by one or more collapse pit craters surrounded by lava outflow lobes (Fig. 14). Except for the region around shield E, the paucity of impact craters large enough to show up in each image suggests relatively recent volcanic activity (e.g., Hauber et al., 2011).

Volcanic structures associated with each shield in Fig. 12 provide details of how well the Earth analogs are suited for comparative geology, and the importance of eruptive fissures rather than central vents on Mars. For example, lava outflow channels and flow lobes from two summit pit craters in shield A (~200 km east of Pavonis Mons), typical plains-style features, clearly indicate topographic control. A well-defined margin representing a change in topography on the west flank further indicates the coalescence of low shields described by Greeley (1977), an important plains-style feature on the ESRP (e.g., Kuntz, 1992; Kuntz et al., 1992; Hughes et al., 1999, 2002a; Miller and Hughes, 2009; Wetmore et al., 2009). Double vents and numerous lava outflow lobes are also recognized in shield B (~260 km south of Pavonis Mons) reflecting a buried fissure system. Although a direct association with a well-defined fissure system is not evident in either A or B low shields, the proximity of two elongate vents provides likely fissure orientation. More direct evidence of fissure eruption is exhibited by a series of several vents on shield C (~430 km E of Arsia Mons) along an obvious fissure, which continues eastward into a series of vents related to an adjacent coalescent shield.

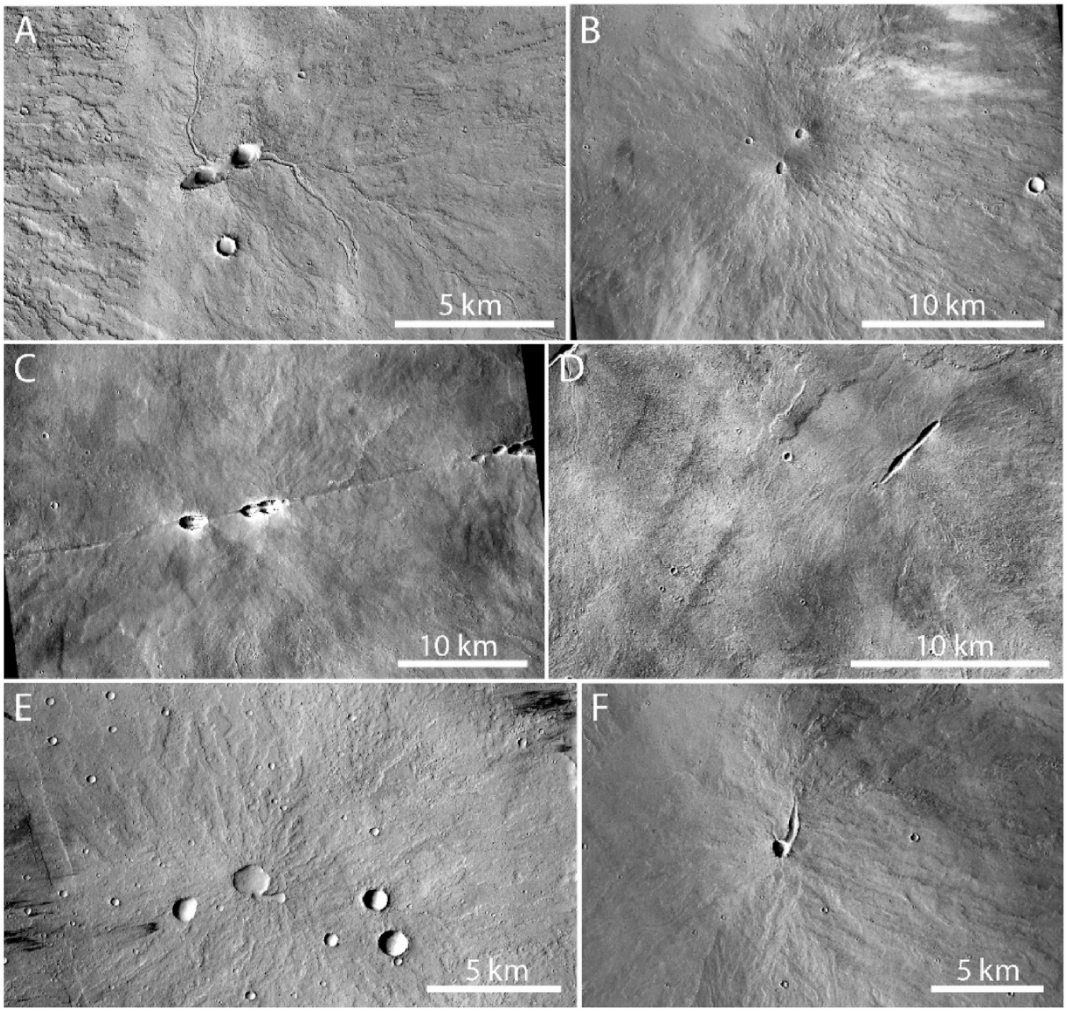

Fig. 13. Representative low shields on Mars listed with CTX image identifiers and locations. A = ID B11_013905_1809_XI_00N109W, Lat 0.94°, Lon 250.26°(-109.74), ~200 km E of Pavonis Mons caldera center; B = ID B11_014037_1761_XN_03S113W, Lat −3.95°, Lon 246.76° (−113.24), ~260 km S of PM caldera; C = ID D05_029320_1723_XI_07S113W, Lat −7.8°, Lon 246.78° (−113.22), ~430 km E of Arsia Mons caldera center; D = ID D22_035702_1773_XN_02S113W, Lat −2.79°, Lon 246.64° (−113.36), ~210 km S of PM caldera center; E = ID P20_008934_2081_XN_28N117W, Lat 28.18°, Lon 242.38° (−117.62), midway between Olympus Mons and Alba Mons; F = ID D07_030098_1748_XI_05S114W, Lat −5.22°, Lon 245.87° (−114.13), ~430 km NE of Arsia Mons caldera.

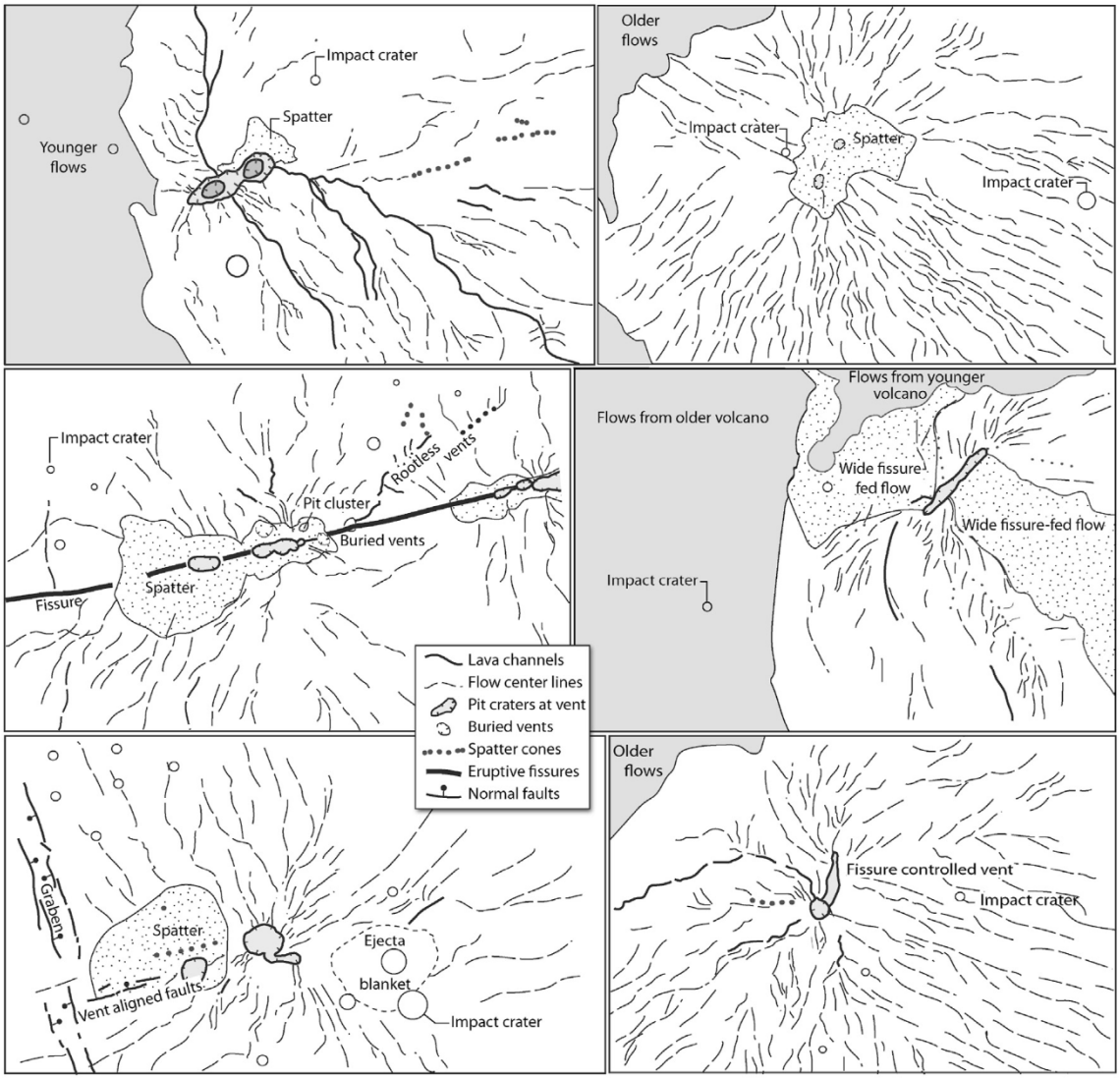

Fig. 14. Sketch maps of low shields on Mars depicted in Fig. 13.

Also, the ~4 km-long vent in shield D (~210 km S of Pavonis Mons) strongly indicates fissure orientation although, as with A and B, any fissure extensions beyond the vent have been obscured by lava lobes. Additional evidence of fissure direction is apparent in the prominent lava lobes on the NW flank of shield D that appear to be deflected north and south by topographic control (and overrun by thick flows from the north), while rough-surfaced lava lobes SE of the vent clearly flowed downslope perpendicular to the fissure.

Some surficial features, such as those in Fig. 13E and F, could possibly lead to misinterpreting low shield developments. For example, volcano E (SW of Alba Mons) exhibits good exposure of lava flow lobes that appear to have flowed northwest and southeast of the vent, which indicate topographic control perpendicular to a SW – NE fissure system at higher elevation. Other features complicate this scenario. First, a prominent graben apparent on the western flank of the shield has the same general orientation as lava flow lobes, which must be considered when interpreting regional stresses or tectonic processes. Second, several post-eruption impact craters (with sizes similar to the summit pit crater) occur on the flanks of the volcano. Although these craters are easily distinguished from the volcanic vent, their impact ejecta possibly obscures volcanic structures, especially outflow lobes that may help interpret fissure orientation. Vent patterns themselves on low shields may also complicate fissure interpretation. The irregular vent on shield F (~430 km NE of Arsia Mons) is typical of many on the Tharsis plains, which have collapse pits and proximal lava channels with unusual morphology (e.g., see Bleacher et al., 2009; Hauber et al., 2009). The example in this shield is notable because the channel is large and oriented in a direction that may indicate a fissure, while the main part of the circular pit crater remains mostly intact.

Volcanic fissures related to the regional fossae surrounding Alba Mons, many within grabens, are apparently related to both magmatic and tectonic forces (Cailleau et al., 2003). Extensive grabens measuring hundreds of km long in the Tharsis region, with or without the surface manifestations of fissure vents, are interpreted as the structural response to the intrusion of large dikes arrested below the surface (e.g., Mège and Masson, 1996; Scott et al., 2002; Wilson and Head, 2002). This interpretation is consistent with Earth analogs and models that depict similar scenarios of dike-induced extension (Pollard et al., 1983; Mastin and Pollard, 1988; Rubin, 1992), as well as models for lunar graben formation (Head and Wilson, 1993) and lunar collapse pits along Rima Hyginus (Wilson et al., 2011). Analogs on Earth such as Kings Bowl support the magmatic interpretation of fossae and graben formation at Alba Mons as implied in Fig. 2 above. Like Kings Bowl, dike intrusion without concomitant low shield growth or extensive lava flows is evident in structures such as vents with possible pyroclastic deposits, collapse or explosion pits, and extension cracks, faults or grabens. However, the

question of whether or not such features on Mars can be considered in our scheme of fissure vent types becomes one of whether or not volcanic deposits can be directly associated with these features.

Of many examples, two representative grabens found in CTX imagery are depicted in Fig. 15. Although without evidence of volcanic eruption, they exhibit dike-induced extension cracks, faults, and grabens. Few if any direct associations of vents to lava flows or pyroclastic deposits are evident, even if lava flows are apparently contemporaneous with graben structures (Fig. 2). Lava flows portrayed in many CTX images of fossae indicate flow directions perpendicular to the linear structures, but the structural features crosscut older lava flows. On the NW flank of Alba Mons, lava flows (Fig. 15A) appear to have an eruptive source along a fissure; yet, close inspection reveals that most, if not all, of these flows have been faulted. Moreover, grabens in Cyane Fossae (Fig. 15B) clearly post-date an older lava flow visible west of the pit-crater chain (see Fig. 2 for comparison). Examples of similar extensional systems are the pit-crater chains in radial and concentric patterns on the flanks of Ascraeus Mons (Pozzobon et al., 2015), which are attributed to normal faulting and feeder dikes. Although these features are the surface expressions of sub-volcanic processes, there is little evidence for fissure eruptions. Thus, it is not possible to designate fissure vent types to any of the numerous fossae-graben or pit-crater chain systems around Alba Mons or in other parts of the Tharsis region. Indeed, one interpretation of Alba Mons grabens that encompass concomitant pit-crater chains is consistent with the detailed assessments of magmatism (Turtle and Melosh, 1997; Scott et al., 2002; Ivanov and Head, 2006) in that they represent the youngest magmatic/tectonic event. They appear as stage IV grabens (Tanaka, 1990) on older extensive lava plains, which were possibly emplaced by type 4 fissure systems comprising the flanks of Alba Mons.

Volcanic surficial features in the Tharsis region of Mars are thus mostly type 2 low shields, and illustrate the latest activity following the growth of the large Tharsis montes. Some of them may retain transitional type 1 characteristics where the eruptive fissure has not been completely obscured. Extension cracks and grabens associated with fossae around Alba Mons display surface features that might be related to dike injection; however, most do not appear to have vents as the sources of either pyroclastic ejecta or lava flows.

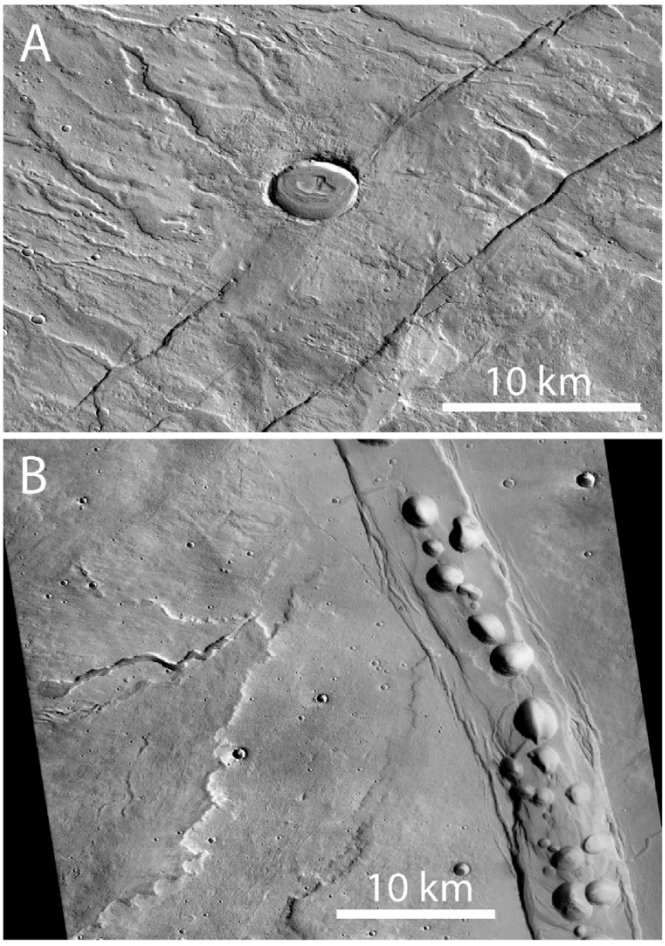

Fig. 15. Representative CTX images of fossae and related features surrounding Alba Mons, Mars. A = ID K03_054598_2248_XN_44N114W, Lat 44.89°, Lon 245.83° (−114.17), NW region of Alba Fossae, NW flank of Alba Mons; B = ID J03_045922_2167_XN_36N118W, Lat 36.73°, Lon 241.5° (−118.5), in Cyane Fossae region, western flank of Alba Mons.

5. Summary – fissure types on the Moon and Mars

The study of volcanic fissure vents on the Moon and Mars, being much older than analogs on Earth, depends on how well they hold up under the processes of surface degradation over geologic time. Those that have not been obscured by subsequent volcanic deposits are subject to secondary processes of impact cratering and regolith formation on both Moon and Mars, and also by the atmospheric effects of erosion, transport and deposition on Mars. Although the detailed examination of relatively young volcanism on either body is hampered by the paucity of fresh exposures, an initial assignment of fissure type in many regions (at the scale of currently available imagery) allows an assessment of geologic setting based on terrestrial analogs. Surface expressions and the dimensions of eruptive fissures, as well as inferences made from related structures, indicate that many visible vents and craters reflect dike-fed eruptions or arrested dike intrusions.

Each terrain, with few exceptions, exhibits a dominant fissure vent landform that can be associated to an Earth analog. Lunar FFCs and mare-like terrains have mostly simple type 1 (monogenetic) fissure vents. Volcanic plains of the greater Tharsis region on Mars are dominated by type 2 monogenetic low shields. Types 3 and 4 polygenetic volcanic rift zones are scarce. Only one type 3 rift is observed on the Moon (Rima Reiko), although more may be found at some point in complex volcanic terrains such as the Mairan, Marius, Gruithuisen and Hortensius domes (Weitz and Head, 1999; Heather et al., 2003; Wilson and Head, 2003; Campbell et al., 2009; Jolliff et al., 2011; Besse et al., 2011; Glotch et al., 2011; Spudis et al., 2013; Lawrence et al., 2013; Ivanov et al., 2016; McBride et al., 2018). Polygenetic type 4 (dike swarm) fissure systems, comprising numerous (now buried) individual type 1 or 2 fissure vents, are believed to have existed on the Moon as mare basalt sources and on Mars as feeder vents during the growth of Alba Mons and other large Tharsis volcanoes.

Basaltic type 1 monogenetic fissures on the Moon are significantly different from their Earth analogs. Typically they are deep and the floors lie well below the surrounding surface; thin non-juvenile pyroclastic dark halo deposits due to vulcanian explosions are characteristic. Exceptions include two type 1 systems in mare terrains with cone profiles (Fig. 11) similar to Earth analogs: Lacus Veris and companions Osiris and Isis. The latter, with stark resemblance to plains volcanism on the ESRP, produced small juvenile spatter or lava cones along Rima Reiko, a complex, possibly type 3 polygenetic rille. Other type 1 vents on major rille complexes (rimae) may be the components of abundant type 4 compound fissure systems.

Type 2 fissures on Mars are quite similar to their Earth analogs. Representative low shields, abundant type 2 features, are clearly associated with elongate vents with evidence of topographic control on outflow lava lobes. Few have visible linear fissures depicting a transitional type 1-to-2 system. They are primary components of plains-style volcanism due to scattered small magma batches, as opposed to much more voluminous magmatism associated with tholi, paterae, and major Tharsis shields. A conundrum is apparent in the fossae around Alba Mons, which contain grabens with collapse pits, extension cracks and

non-eruptive fissures, all typical structures of type 1 fissures. Although related to internal magma-driven processes, they crosscut older lavas and cannot be strictly classified as type 1 fissures.

The preponderance of types 1 and 2 systems reflect the latest stages of volcanism on both bodies subsequent to major episodes of planetary evolution, i.e., deep-sourced mare basalts on the Moon and the growth of large volcanoes on Mars. A tentative implication of these observations is that the prodigious magmatism that produced mare basalts on the Moon and large shields on Mars are intrinsically separate from the later episodes of less voluminous magma production. Magmatic processes related to FFC and cryptomare dike injections, and low shield eruptions (at least those in the Tharsis region) seem to represent completely separate systems without significant transitional episodes. Apparently, the more recent events, compared to previous lava outpourings, were simple eruptions from small magma bodies without significant volumes of either tephra or lava. Profiles measured across fissures on the Moon and the scales of low shields on Mars further imply that FFC and low shield fissures are generally smaller than fissures on mare rilles or the vents (including calderas) that produced the great Tharsis volcanoes. Thus, it may be inferred that FFC and low-shield eruptions were derived from relatively low magma volumes compared to lunar mare and major shield systems on Mars.

6. Conclusions

The proposed designation of eruptive fissure types 1–4, based on Earth examples, provides a preliminary classification for the evaluation of extraterrestrial volcanic processes. The classification can be used to establish the fundamental architecture of fissure systems on other planets, although the types must be broadly defined in order to include myriad variants. More importantly, only the simpler types 1 and 2 are believed to exist in abundance on the surfaces of the Moon and Mars; whereas, types 3 and 4 are either scarce or inferred. Unlike either type 1 or 2, type 3 fissures require knowledge of compositional varieties as well as polygenetic eruptions. Type 4 fissure vents require knowledge of an association to voluminous flood lavas and a regional network of fissures, regardless of whether individual fissures are type 1 (monogenetic) or type 3 features.

The preponderance of type 1 fissure vents in lunar FFCs is consistent with recent discoveries and models that indicate eruption from relatively small, localized magma reservoirs, mainly shallow sills and laccoliths fed by dikes that originate from deeper sources. The primary difference between FFC fissures and Earth analogs is that most FFC deposits appear to represent vulcanian-style explosive eruptions of non-juvenile blocks rather than eruptions of fluid lava. Type 1 fissures are also observed in mare and cryptomare terrains, yet their association with long rilles in complex rimae systems indicates deep-sourced type 4 dike swarms related to mare basalts that covered most vents. Type 2 vents are scarce in the regions reviewed on the Moon although they are common as low shields on Mars. Type 3 systems, numerous on Earth, are represented in only one lunar mare terrain; yet future studies may identify others on the Moon and Mars. Extensive mare basalts and lava flows on the flanks of large Tharsis shields and surrounding plains may indicate development from type 4 dike swarms; however, those associations will require more detailed exploration.

Author Contributions

Scott Hughes – Conceptualization, Investigation, Formal Analysis, Writing. Brent Garry – Conceptualization, Investigation, Methodology, Validation, Writing. Alexander Sehlke – Investigation, Validation, Writing. Eric Christiansen – Investigation, Writing, Validation. Shannon Nawotniak – Investigation, Validation. Derek Sears – Investigation, Validation. Richard Elphic – Investigation, Validation

Declaration of competing interest

The authors declare that they have no known competing financial interests or personal relationships that could have appeared to influence the work reported in this paper.

Acknowledgements

Craters of the Moon National Monument and Preserve and surrounding volcanic terrains on the eastern Snake River Plain, are primary targets of NASA project FINESSE (Field Investigations to Enable Solar System Science and Exploration). Support for this project was provided by FINESSE, NASA grant number NNX14AG35A to Jennifer L. Heldmann, PI, through the Solar System Exploration Research Virtual Institute (SSERVI). The authors thank all FINESSE team members for assistance in field work and data compilation. Comprehensive reviews by Jim Head and an anonymous reviewer significantly improved the manuscript, although the authors take full responsibility for any misinterpretations or misrepresentations.

References

Armstrong, R.L., Leeman, W.P., Malde, H.E., 1975. K-Ar dating, quaternary and neogene volcanic rocks of the Snake River plain, Idaho. Am. J. Sci. 275, 225–251.

Audin, J., Vellutini, P.J., Coulon, C., Piguet, P., Vincent, J., 1990. The 1928-1929 eruption of Kammourta volcano - evidence of tectono-magmatic activity in the Manda-Inakir rift and comparison with the Asal Rift, Afar depression, Republic of Djibuti. Bull. Volcanol. 52, 551–561.

Bamberg, M., Jauman, R., Asche, H., Kneissl, T., Michael, G.G., 2014. Floor-fractured craters on Mars – observations and origin. Planet. Space Sci. 98, 146–162.

Barberi, F., Varet, J., 1977. Volcanism of Afar: small-scale plate tectonics implications. Geol. Soc. Am. Bull. 88, 1251–1266.

Barker, M.K., Mazarico, E., Neumann, G.A., Zuber, M.T., Haruyama, J., Smith, D.E., 2015. A new lunar digital elevation model from the lunar orbiter laser altimeter and SELENE terrain Camera. Icarus 273, 346–355.

Besse, S., Sunshine, J.M., Staid, M.I., Petro, N.E., Boardman, J.W., Green, R.O., Head, J.W., Isaacson, P.J., Mustard, J.F., Pieters, C.M., 2011. Compositional variability of the Marius hills volcanic complex from the Moon mineralogy mapper (M3). J. Geophys. Res. 116 https://doi.org/10.1029/2010JE003725. E00G13.

Bleacher, J.E., Glaze, L.S., Greeley, R., Hauber, E., Baloga, S.M., Sakimoto, S.E.H., Williams, D.A., Glotch, T.D., 2009. Spatial and alignment analyses for a field of small volcanic vents south of Pavonis Mons and implications for the Tharsis province, Mars. J. Volcanol. Geoth. Res. 185, 96–102.

Braden, S.E., Stopar, J.D., Robinson, M.S., Lawrence, S.J., van der Bogert, C.H., Hiesinger, H., 2014. Evidence for basaltic volcanism on the Moon within the past 100 million years. Nat. Geosci. 7 (11), 787–791. https://doi.org/10.1038/NGEO2252.

Brož, P., Hauber, E., 2013. Hydrovolcanic tuff rings and cones as indicators for phreatomagmatic explosive eruptions on Mars. J. Geophys. Res. Planets 118, 1656–1675. https://doi.org/10.1002/jgre.20120.

Cahill, J.T.S., Thomson, B.J., Patterson, G.W., Bussey, D.B.J., Neish, C.D., Lopez, N.R., Turner, F.S., Aldridge, T., McAdam, M., Meyer, H.M., Raney, R.K., Carter, L.M., Spudis, P.D., Hiesinger, H., Pasckert, J.H., 2014. The miniature radio frequency instrument's (Mini-RF) global observations of Earth's Moon. Icarus 243, 173–190.

Cailleau, B., Walter, T.R., Janle, P., Hauber, E., 2003. Modeling volcanic deformation in a regional stress field: implications for the formation of graben structures on Alba Patera, Mars. J. Geophys. Res. 108 (E12), 5141. https://doi.org/10.1029/2003JE002135.

Campbell, B.A., Hawke, B.R., Campbell, D.B., 2009. Surface morphology of domes in the Marius hills and Mons rümker regions of the Moon from earth-based radar data. J. Geophys. Res. 114, E01001. https://doi.org/10.1029/2008JE003253.

Carr, M.H., 1973. Volcanism on Mars. J. Geophys. Res. 78 (20), 4049–4062.

Carr, M.H., Head, J.W., 2010. Geologic history of Mars. Earth Planet Sci. Lett. 294 (3), 185–203.

Carter, L.M., Campbell, B.A., Hawke, B.R., Campbell, D.B., Nolan, M.C., 2009. Radar remote sensing of pyroclastic deposits in the southern Mare Serenitatis and Mare Vaporum regions of the Moon. J. Geophys. Res. 114, E11004. https://doi.org/10.1029/2009JE003406.

Carter, L.M., Petro, N.E., Campbell, B.A., Baker, D.M.H., Morgan, G.A., 2017. Earth-based radar and orbital remote sensing observations of mare basalt flows and pyroclastic deposits in Mare Nubium. Lunar Planet. Sci. XLVIII abstract #1736.

Delano, J.W., 1986. Pristine lunar glasses: criteria, data, and implications. In: Proc. Lunar Planet. Sci. Conf. 16th, vol. 91, pp. D201–D213. J. Geophys. Res.

Gaddis, L.R., Pieters, C.M., Hawke, B.R., 1985. Remote sensing of lunar pyroclastic mantling deposits. Icarus 61, 461–489.

Gaddis, L.R., Hawke, B.R., Robinson, M.S., Coombs, C., 2000. Compositional analyses of small lunar pyroclastic deposits using Clementine multispectral data. J. Geophys. Res. B 105, 4245–4262.

Gaddis, L.R., Staid, M.I., Tyburczy, J.A., Hawke, B.R., Petro, N.E., 2003. Compositional analyses of lunar pyroclastic deposits. Icarus 161, 262–280. https://doi.org/10.1016/S0019-1035(02)00036-2.

Garry, W.B., Robinson, M.S., Zimbelman, J.R., Bleacher, J.E., Hawke, B.R., Crumpler, L.S., Braden, S.E., Sato, H., 2012. The origin of Ina: evidence for inflated lava flows on the Moon. J. Geophys. Res. 117, E00H31. https://doi.org/10.1029/2011JE003981.

Global Volcanism Program, 2013. Volcanoes of the world, v. 4.7.5. In: Venzke, E. (Ed.), Smithsonian Institution. https://doi.org/10.5479/si.GVP.VOTW4-2013. Downloaded 06 Jan 2019.

Glotch, T.D., Hagerty, J.J., Lucey, P.G., et al., 2011. The Mairan domes: silicic volcanic constructs on the Moon. Geophys. Res. Lett. 38, L21204. https://doi.org/10.1029/2011GL049548.

Greeley, R., King, J.S., 1977. In: Volcanism of the Eastern Snake River Plain, Idaho: A Comparative Planetary Geology Guidebook. NASA Contract. Rep., p. 308. CR-154621.

Greeley, R., 1977. Basaltic "plains" volcanism. In: Greeley, R., King, J.S. (Eds.), Volcanism Of the Eastern Snake River Plain, Idaho: A Comparative Planetary Geology Guidebook. NASA Contract. Rep., pp. 24–44. CR-154621.

Greeley, Ronald, 1982. The Snake River plain, Idaho: representative of a new category of volcanism. J. Geophys. Res. B 87, 2705–2712.

Greeley, R., Schultz, P.H., 1977. Possible planetary analogs to Snake River plain basalt features. In: Greeley, R., King, J.S. (Eds.), Volcanism Of the Eastern Snake River Plain, Idaho: A Comparative Planetary Geology Guidebook. NASA Contract. Rep., pp. 233–251. CR-154621.

Greeley, R., Theilig, E., King, J.S., 1977. Guide to the geology of King's Bowl lava field. In: Greeley, R., King, J.S. (Eds.), Volcanism Of the Eastern Snake River Plain, Idaho: A Comparative Planetary Geology Guidebook. NASA Contract. Rep., pp. 171–188. CR-154621.

Gudmundsson, Agust, 2003. Surface stresses associated with arrested dykes in rift zones. Bull. Volcanol. 65, 606–619.

Gustafson, J.O., Bell III, J.F., Gaddis, L.R., Hawke, B.R., Giguere, T.A., 2012. Characterization of previously unidentified lunar pyroclastic deposits using Lunar Reconnaissance Orbiter Camera data. J. Geophys. Res. 117 https://doi.org/10.1029/2011JE003893. E00H25.

Hauber, E., Bleacher, J.E., Gwinner, K., Williams, D.A., Greeley, R., 2009. The topography and morphology of low shields and associated landforms of plains volcanism in the Tharsis region of Mars. J. Volcanol. Geoth. Res. 185, 69–95.

Hauber, E., Brož, P., Jagert, F., Jodłowski, P., Platz, T., 2011. Very recent and wide-spread basaltic volcanism on Mars. Geophys. Res. Lett. 38, L10201. https://doi.org/10.1029/2011GL047310.

Hawke, B.R., Coombs, C.R., Gaddis, L.R., Lucey, P.G., Owensby, P.D., 1989. Remote sensing and geologic studies of localized dark mantle deposits on the Moon. Proc. Lunar Planet Sci. Conf. 19th, 255–268.

Hawke, B.R., Giguere, T.A., Peterson, C.A., Lawrence, S.J., Stopar, J.D., Gaddis, L.R., 2015. Cryptomare, lava lakes, and pyroclastic deposits in the Gassendi region of the Moon: final results. In: *46th Lunar And Planetary Science Conference* abstract #1310.

Head, J.W., 1974. Lunar dark mantle deposits: possible clues to the distribution of early mare deposits. In: Proc. Lunar Sci. Conf. 5th, pp. 207–222.

Head, J.W., Coffin, M.F., 1997. Large igneous provinces: a planetary perspective. In: Mahoney, J.J., Coffin, M.F. (Eds.), Large Igneous Provinces: Continental, Oceanic, and Planetary Flood Volcanism, vol. 100. American Geophysical Union *Geophysical Monograph*, pp. 411–438.

Head, J.W., Wilson, L., 1979. Alphonsus-type dark-halo craters: morphology, morphometry, and eruption conditions. Proc. Lunar Planet Sci. Conf. 10th, 2861–2897.

Head, J.W., Wilson, L., 1991. Absence of large shield volcanoes and calderas on the Moon: consequence of magma transport phenomena? Geophys. Res. Lett. 18 (11), 2121–2124.

Head, J.W., Wilson, L., 1992. Lunar mare volcanism: stratigraphy, eruption conditions, and the evolution of secondary crusts. Geochem. Cosmochim. Acta 56, 2155–2175.

Head, J.W., Wilson, L., 1993. Lunar graben formation due to near-surface deformation accompanying dike emplacement. Planet. Space Sci. 41, 719–727.

Head, J.W., Wilson, L., 2017. Generation, ascent and eruption of magma on the Moon: new insights into source depths, magma supply, intrusions and effusive/explosive eruptions (Part 2: predicted emplacement processes and observations). Icarus. https://doi.org/10.1016/j.icarus.2016.05.031.

Head, J.W., Wilson, L., Weitz, C.M., 2002. Dark ring in southwestern Orientale Basin: origin as a single pyroclastic eruption. J. Geophys. Res. 107 (E1) https://doi.org/10.1029/2000JE001438.

Heather, D.J., Dunkin, S.K., Wilson, L., 2003. Volcanism on the Marius Hills plateau: observational analyses using Clementine multispectral data. J. Geophys. Res. 108 (E3), 5017. https://doi.org/10.1029/2002JE001938.

Henderson, A.O., Christiansen, E.H., Radebaugh, J., 2015. Low-shield volcanism: a comparison of volcanoes on Syria Planum, Mars and Snake River plain, Idaho. In: 46th Lunar And Planetary Science Conference. Abstract 2685.

Heiken, G.H., McKay, D.S., Brown, P.W., 1974. Lunar deposits of possible pyroclastic origin. Geochem. Cosmochim. Acta 38, 1703–1718.

Hiesinger, H., Head, J.W., 2006. New views of lunar geoscience: an introduction and overview. In: Jolliff, B., Wiezcorek, M. (Eds.), New Views of the Moon, *Reviews In Mineralogy And Geochemistry, 60*. Mineralogical Society of America, pp. 1–81.

Hiesinger, H., Head, J.W., Wolf, U., et al., 2011. Ages and stratigraphy of lunar mare basalts: a synthesis. In: Ambrose, W.A., Williams, D.A. (Eds.), Recent Advances and Current Research Issues in Lunar Stratigraphy. *Geol. Soc. Am. Special Paper*, vol. 477, pp. 1–51.

Hodges, C.A., 1979. Some Lesser Volcanic Provinces on Mars. Reports of Planetary Geology Program. NASA TM-80339, Washington, D.C., pp. 247–249, 1978–1979.

Hodges, C.A., Moore, H.J., 1994. Atlas of volcanic landforms on Mars. U. S. Geol. Surv. Prof. Pap. 1534, 194 (with map).

Holmes, A.A.J., Rodgers, D.W., Hughes, S.S., 2008. Kinematic analysis of fractures in the Great Rift, Idaho: implications for subsurface dike geometry, crustal extension, and magma dynamics. J. Geophys. Res. B 113, B04202. https://doi.org/10.1029/2006JB004782.

Hughes, S.S., Smith, R.P., Hackett, W.R., Anderson, S.R., 1999. Mafic volcanism and environmental geology of the eastern Snake River Plain. In: Hughes, S.S., Thackray, G.D. (Eds.), Guidebook to the Geology of Eastern Idaho. Idaho Museum of Natural History, pp. 143–168.

Hughes, S.S., McCurry, M., Geist, D.J., 2002. Geochemical correlations and implications for the magmatic evolution of basalt flow groups at the Idaho National Engineering and Environmental Laboratory. In: Link, P.K., Mink, L.L. (Eds.), Geology, Hydrogeology and Environmental Remediation, Idaho National Engineering and Environmental Laboratory, Eastern Snake River Plain. Geol. Soc. Am. Special Paper, vol. 353, pp. 151–173.

Hughes, S.S., Kobs Nawotniak, S.E., Sears, D.W.G., Garry, W.B., Haberle, C.W., Bleacher, J.E., Lim, D.S.S., Heldmann, J.L., the Finesse Team, 2015. King's Bowl, Idaho – a volcanic analog for fissure eruptions, pit craters and dike injection along Rima Hyginus, Moon, and Cyane Fossae, Mars. In: *46th Lunar And Planetary Science Conference* abstract #2846.

Hughes, S.S., Garry, W.B., Kobs Nawotniak, S.E., Sehlke, A., Christiansen, E.H., Lim, D.S.S., Heldmann, J.L., 2017. Geochemical diversity within monogenetic basaltic systems may be magmatic analogs for small-scale intrusions in floor-fractured craters. In: *48th Lunar And Planetary Science Conference* abstract #2628.

Hughes, S.S., Kobs Nawotniak, S.E., Sears, D.W.G., Borg, C., Garry, W.B., Christiansen, E.H., Haberle, C.W., Lim, D.S.S., Heldmann, J.L., 2018. Phreatic explosions during basaltic fissure eruptions: Kings Bowl lava field, Snake River Plain, USA. J. Volcanol. Geoth. Res. 351, 89–104.

Hurwitz, D.M., Head, J.W., Hiesinger, H., 2013. Lunar sinuous rilles: distribution, characteristics, and implications for their origin. Planet. Space Sci. 79–80, 1–38.

Ivanov, M.A., Head, J.W., 2006. Alba Patera, Mars: topography, structure, and evolution of a unique late Hesperian–early Amazonian shield volcano. J. Geophys. Res. 111, E09003. https://doi.org/10.1029/2005JE002469.

Ivanov, M.A., Head, J.W., Bystrov, A., 2016. The lunar Gruithuisen silicic extrusive domes: topographic configuration, morphology, ages, and internal structure. Icarus 273, 262–283. https://doi.org/10.1016/j.icarus.2015.12.015.

Jenness, M.H., Clifton, A.E., 2009. Controls on the geometry of a Holocene crater row: a field study from southwest Iceland. Bull. Volcanol. 71, 715-528.

Jolliff, B.L., Gillis, J.J., Haskin, L.A., Korotev, R.L., Wieczorek, M.A., 2000. Major lunar crustal terranes: surface expressions and crust-mantle origins. J. Geophys. Res. 105, 4197–4216.

Jolliff, B.L., Wiseman, S.A., Lawrence, S.J., et al., 2011. Non-mare silicic volcanism on the lunar farside at Compton–Belkovich. Nat. Geosci. 4, 566–571.

Jozwiak, L.M., Head, J.W., Zuber, M.T., Smith, D.E., Neumann, G.A., 2012. Lunar floor-fractured craters: classification, distribution, origin and implications for magmatism and shallow crustal structure. J. Geophys. Res. 117, E11.

Jozwiak, L.M., Head, J.W., Wilson, L., 2015. Lunar floor-fractured craters as magmatic intrusions: geometry, modes of emplacement, associated tectonic and volcanic features, and implications for gravity anomalies. Icarus 248, 424–447.

Jozwiak, L.M., Head, J.W., Neumann, G.A., Wilson, L., 2017. Observational constraints on the identification of shallow lunar magmatism: insights from floor-fractured craters. Icarus 283, 224–231.

Keszthelyi, L., Thordarson, T., McEwen, A., Haack, H., Guilbaud, M.N., Self, S., Rossi, M.J., 2004. Icelandic analogs to Martian flood lavas. G-cubed 5, 1–32.

Kuntz, M.A., 1992. A model-based perspective of basaltic volcanism, eastern Snake River Plain, Idaho. In: Link, P.K., Kuntz, M.A., Platt, L.B. (Eds.), Regional Geology of Eastern Idaho and Western Wyoming. Geol. Soc. Am. Memoir, vol. 179, pp. 289–304.

Kuntz, M.A., Covington, H.R., Schorr, L.J., 1992. An overview of basaltic volcanism on the eastern Snake River Plain, Idaho. In: Link, P.K., Kuntz, M.A., Platt, L.B. (Eds.), Regional Geology of Eastern Idaho and Western Wyoming: *Geol.* Soc. Am. Memoir, vol. 179, pp. 227–267.

Kuntz, M.A., Anderson, S.R., Champion, D.E., Lanphere, M.A., Grunwald, D.J., 2002. Tension cracks, eruptive fissures, dikes, and faults related to the Pleistocene-Holocene basaltic volcanism and implications for the distribution of hydraulic conductivity in the eastern Snake River Plain, Idaho. In: Link, P.K., Mink, L.L. (Eds.), Geology Hydrogeology, and Environmental Remediation: Idaho National Engineering and Environmental Laboratory, Eastern Snake River Plain, Idaho. Geol. Soc. Am. Special Paper, vol. 353, pp. 111–133.

Kuntz, M.A., Skipp, Betty, Champion, D.E., Gans, P.B., Van Sistine, D.P., Snyders, S.R., 2007. Geologic map of the Craters of the Moon 30' x 60' quadrangle, Idaho. U.S. Geol. Surv. Sci. Invest. Map 2969, 64 pamphlet, 1 plate, scale 1:100,000.

Lawrence, S.J., et al., 2013. LRO observations of morphology and surface roughness of volcanic cones andlobate lava flows in the Marius Hills. J. Geophys. Res. Planets 118, 615–634. https://doi.org/10.1002/jgre.20060.

Lockwood, J.P., Tilling, R.I., Holcomb, R.T., Klein, F., Okamura, A.T., Peterson, D.W., 1999. Magma migration and resupply during the 1974 summit eruptions of Kilauea Volcano, Hawai'i. U.S. Geol. Surv. Prof. Pap. 1613, 37.

Malin, M.C., et al., 2007. Context Camera investigation on board the Mars reconnaissance orbiter. J. Geophys. Res. 112, E05S04. https://doi.org/10.1029/2006JE002808.

Mastin, L.G., Pollard, D.D., 1988. Surface deformation and shallow dike intrusion processes at Inyo Craters, Long Valley, California. J. Geophys. Res. B 93 (13), 221-13,236.

McBride, M.J., Horgan, B.H.N., Lawrence, S.J., 2018. Spectral analysis of lunar cinder cones in the Marius Hills volcanic complex. In: 49th *Lunar And Planet. Sci. Conf.* abstract #2798.

Mège, D., Masson, P., 1996. Stress models for Tharsis formation, Mars. Planet. Space Sci. 44, 1499–1546.
Mège, D., Korme, T., 2004. Dyke swarm emplacement in the Ethiopian Large Igneous Province: not only a matter of stress. J. Volcanol. Geoth. Res. 132, 283–310.
Mège, D., Cook, A.C., Garel, E., Lagabrielle, Y., Cormier, M.-H., 2003. Volcanic rifting at Martian grabens. J. Geophys. Res. 108 (E5), 5044. https://doi.org/10.1029/2002JE001852.
Miller, M.L., Hughes, S.S., 2009. Mixing primitive and evolved olivine tholeiite magmas in the eastern Snake River Plain, Idaho. J. Volcanol. Geoth. Res. 188, 153–161.
Mohr, P.A., Wood, C.A., 1976. Volcano spacings and lithospheric attenuation in the eastern rift of Africa. Earth Planet Sci. Lett. 33, 126–144.
Moore, H.J., Hodges, C.A., 1980. Some Martian Volcanic Centers with Small Edifices. Reports of Planetary Geology Program-1988, pp. 266–268. NASA-TM 82385, Washington, D.C.
Neal, C.A., Lockwood, J.P., 2003. Geologic map of the summit region of Kīlauea volcano, Hawai'i. *U.S. Geol. Surv. Geol. Invest.Series* I-2759. Scale = 1:24,000.
Neal, C.R., Taylor, L.A., 1992. Petrogenesis of mare basalts: a record of lunar volcanism. Geochem. Cosmochim. Acta 56, 2177–2211.
Needham, D., Choukroune, P., Cheminée, J.L., Le Pichon, X., Francheteau, J., Tapponier, P., 1976. The accreting plate boundary: Ardoukoba rift (Northeast Africa) and the oceanic rift valley. Earth Planet Sci. Lett. 28, 439–453.
Orr, T., Heliker, C., Patrick, M., 2012. The ongoing Pu'u 'O'ō eruption of Kīlauea Volcano, Hawai'i—30 years of eruptive activity. U.S. Geol. Suev. Fact Sheet 6, 2012-3127.
Peters, S.I., Christensen, P.R., 2017. Flank vents and graben as indicators of Late Amazonian volcanotectonic activity on Olympus Mons. J. Geophys. Res.: Plan 122 (3), 501–523. https://doi.org/10.1002/2016JE005108.
Petro, N.E., Schmitt, H.H., Hayne, P., Hollibaugh-Baker, D., Moriarty, D., Richardson, H.J., Whelley, P., 2018. Volcanic fissure and associated deposit on the north massif of the Taurus-Littrow Valley: distribution of ash and sample implications. In: *49th Lunar And Planet. Sci. Conf.* abstract #2631.
Pierce, K.L., Morgan, L.A., 1992. The track of the Yellowstone hotspot: volcanism, faulting, and uplift. In: Link, P.K., Kuntz, M.A., Platt, L.P. (Eds.), Regional Geology of Eastern Idaho and Western Wyoming: *Geol.* Soc. Am. Mem., vol. 179, pp. 1–53.
Pieters, C.M., McCord, T.B., Zisk, S.H., Adams, J.B., 1973. Lunar black spots and the nature of the Apollo 17 landing area. J. Geophys. Res. 78, 5867–5875.
Pieters, C.M., McCord, T.B., Charette, M.P., Adams, J.B., 1974. Lunar surface: identification of the dark mantling material in the Apollo 17 soil samples. Science 183, 1191–1194.
Plescia, J.B., 2004. Morphometric properties of Martian volcanoes. J. Geophys. Res. 109, E03003. https://doi.org/10.1029/2002JE002031.
Pollard, D.D., Delaney, P.T., Duffield, W.A., Endo, E.T., Okamura, A.T., 1983. Surface deformation in volcanic rift zones. Tectonophysics 94, 541–584.
Pozzobon, R., Mazzarini, F., Massironi, M., Marinangeli, L., 2015. Self-similar clustering distribution of structural features on Ascraeus Mons (Mars): implications for magma chamber depth. Geol. Soc. London Spec. Publ. 401, 203–218.
Qiao, L., Head III, J.W., Wilson, L., Xiao, L., Dufek, J.D., 2017. Ina pit crater on the Moon: extrusion of waning-stage lava lake magmatic foam results in extremely young crater retention ages. Geology 45, 455–458. https://doi.org/10.1130/G38594.1.
Qiao, L., Head III, J.W., Ling, Z., Wilson, L., Xiao, L., Dufek, J.D., Yan, J., 2019. Geological characterization of the Ina shield volcano summit pit crater on the Moon: evidence for extrusion of waning-stage lava lake magmatic foams and anomalously young crater retention ages. J. Geophys. Res. 124, 1100–1140. https://doi.org/10.1029/2018JE005841.
Richardson, J.A., Wilson, J.A., Connor, C.B., Bleacher, J.E., Kiyosugi, K., 2017. Recurrence rate and magma effusion rate for the latest volcanism on Arsia Mons, Mars. Earth Planet Sci. Lett. 458, 170–178.
Rubin, A.M., 1992. Dike-induced faulting and graben subsidence in volcanic rift zones. J. Geophys. Res. B 97, 1839–1858.
Rubin, A.M., Pollard, D.D., 1988. Dike-induced faulting in rift zones of Iceland and Afar. Geology 16, 413–417.
Sæmundsson, K., Sigurgeirsson, M.Á., Friðleifsson, G.Ó., 2018. Geology and structure of the Reykjanes volcanic system, Iceland. J. Volcanol. Geoth. Res. 11 https://doi.org/10.1016/j.jvolgeores.2018.11.022.
Schmitt, H.H., Petro, N.E., Wells, R.A., Robinson, M.S., Weiss, B.P., Mercer, C.M., 2017. Revisiting the field geology of Taurus-Littrow. Icarus 298, 2–33.
Schultz, P.H., 1976. Floor-fractured lunar craters. Moon 15, 241–273. https://doi.org/10.1007/BF00562240.
Scott, E.D., Wilson, L., Head, J.W., 2002. Emplacement of giant radial dikes in the northern Tharsis region of Mars. J. Geophys. Res. 107 (E2) https://doi.org/10.1029/2000JE001431, 2002.
Sears, D.W.G., Sears, H., Sehlke, A., Hughes, S.S., 2017. Induced thermoluminescence as a method for dating recent volcanism: eastern Snake River Plain, Idaho, USA. J. Geophys. Res. Solid Earth 122, 906–922. https://doi.org/10.1002/2016JB013596.
Sehlke, A., Whittington, A.G., 2020. Rheology of a KREEP analog magma: experimental results applied to dike ascent through the lunar crust. Planet. Space Sci. 187 https://doi.org/10.1016/j.pss.2020.104941.
12 others Shearer, C.K., Hess, P.C., Wieczorek, M.A., Pritchard, M.E., 2006. Thermal and magmatic evolution of the moon. Rev. Mineral. Geochem. 60, 365–518.
Shkuratov, Y.G., Ivanov, M.A., Korokhin, V.V., Kaydash, V.G., Basilevsky, A.T., Videen, G., Hradyska, L.V., Velikodsky, Y.I., Marchenko, G.P., 2018. Characterizing dark mantle deposits in the lunar crater Alphonsus. Planet. Space Sci. 153, 22–38.
Smith, R.B., Braile, L.W., 1994. The Yellowstone hot spot. J. Volcanol. Geoth. Res. 61, 121–187.
Snyder, G.A., Taylor, L.A., Neal, C.R., 1992. A chemical model for generating the sources of mare basalts: combined equilibrium and fractional crystallization of the lunar magmasphere. Geochem. Cosmochim. Acta 56, 3809–3823.
Spudis, P.D., 1999. Volcanism on the moon. In: Sigurdsson, H., et al. (Eds.), Encyclopedia of Volcanoes. Academic Press, San Diego, Calif, pp. 697–708.
Spudis, P.D., McGovern, P.J., Kiefer, W.S., 2013. Large shield volcanoes on the Moon. J. Geophys. Res. Planets 118, 1063–1081. https://doi.org/10.1002/jgre.20059.
Swanson, D.A., Duffield, W.A., Jackson, D.B., Peterson, D.W., 1979. Chronological Narrative of the 1969-1971 Mauna Ulu Eruption of Kīlauea Volcano, Hawai'i. *U.S. Geological Survey Prof. Paper*, p. 55, 1056.
Tanaka, K.L., 1990. Tectonic history of the Alba patera-ceraunius fossae region of Mars. Proc. Lunar Planet Sci. Conf. 20th, 515–523.
Tanaka, K.L., Skinner Jr., J.A., Dohm, J.M., Irwin III, R.P., Kolb, E.J., Fortezzo, C.M., Platz, T., Michael, G.G., Hare, T.M., 2014. Geologic map of Mars: *U.S.* Geol. Surv. Sci. Invest. Map 3292. https://doi.org/10.3133/sim3292 scale 1:20,000,000, pamphlet 43 pp.
Thordarson, T., Self, S., 1993. The Laki (skaftár fires) and grímsvötn eruptions in 1783–1785. Bull. Volcanol. 55, 233–263.
Thorey, C., Michaut, C., 2014. A model for the dynamics of crater-centered intrusion: application to lunar floor-fractured craters. J. Geophys. Res. Planets 119. https://doi.org/10.1002/2013JE004467.
Thorey, C., Michaut, C., Wieczorek, M.A., 2015. Gravitational signatures of lunar floor-fractured craters. Earth Planet Sci. Lett. 424, 269–279.
Tilling, R.I., Heliker, C., Swanson, D.A., 2010. Eruptions of Hawaiian volcanoes— past, present, and future: *U.S.* Geol. Surv. Gen. Inf. Prod 117, 63.
Tilling, R.I., Christiansen, R.L., Duffield, W.A., Endo, E.T., Holcomb, R.T., Koyanagi, R.Y., Peterson, D.W., Unger, J.D., 1987. The 1972-1974 Mauna Ulu eruption, Kīlauea Volcano: an example of quasi-steady-state magma transfer. U. S. Geol. Surv. Prof. Pap. 1350, 405–469.
Turtle, E.P., Melosh, H.J., 1997. Stress and flexural modeling of the Martian lithospheric response to Alba Patera. Icarus 126, 197–211.
Walker, G.P.L., 2000. Basaltic volcanoes and volcanic systems. In: Sigurdsson, H. (Ed.), Encyclopedia of Volcanoes. Academic Press, pp. 283–289.
Weitz, C.M., Head III, J.W., 1999. Spectral properties of the Marius Hills volcanic complex and implications for the formation of lunar domes and cones. J. Geophys. Res. 104 (18), 933-18,959.
Wetmore, P.W., Hughes, S.S., Connor, L.J., Caplinger, M.L., 2009. Spatial distribution of eruptive centers about the Idaho National Laboratory. In: Connor, C.B., Chapman, N.A., Connor, L.J. (Eds.), Volcanic and Tectonic Hazard Assessment for Nuclear Facilities. Cambridge University Press, pp. 385–405 ch. 16.
White, R.S., McKenzie, D.P., 1989. Magmatism at rift zones: the generation of volcanic continental margins and flood basalts. J. Geophys. Res. B 94, 7685–7729.
Wilson, L., Head, J.W., 1981. Ascent and eruption of basaltic magma on the earth and moon. J. Geophys. Res. 86, 2971–3001.
Wilson, L., Head, J.W., 1994. Mars: review and analysis of volcanic eruption theory and relationships to observed landforms. Rev. Geophys. 32, 221–263.
Wilson, L., Head, J.W., 2002. Tharsis-radial graben systems as the surface manifestation of plume-related dike intrusion complexes: models and implications. J. Geophys. Res. B 107 (E8), 10.11-029/2001JE001593.
Wilson, L., Head, J.W., 2003. Lunar gruithuisen and mairan domes: rheology and mode of emplacement. J. Geophys. Res. 108 https://doi.org/10.1029/2002JE001909.
Wilson, L., Head III, J.W., 2017. Eruption of magmatic foams on the Moon: formation in the waning stages of dike emplacement events as an explanation of "irregular mare patches". J. Volcanol. Geoth. Res. 335, 113–127. https://doi.org/10.1016/j.jvolgeores.2017.02.009.
Wilson, L., Head, J.W., 2018a. Lunar floor-fractured craters: modes of dike and sill emplacement and implications of gas production and intrusion cooling on surface morphology and structure. Icarus 305, 105–122.
Wilson, L., Head III, J.W., 2018b. Controls on lunar basaltic volcanic erupton structure and morphology: gas release patterns in sequential eruption phases. Geophys. Res. Lett. 45, 5852–5859. https://doi.org/10.1029/2018GL078327.
Wilson, L., Mouginis-Mark, P.J., Tyson, S., Mackown, J., Garbeil, H., 2009. Fissure eruptions in Tharsis, Mars: implications for eruption conditions and magma sources. J. Volcanol. Geoth. Res. 185, 28–46.
Wilson, L., Hawke, B.R., Giguere, T.A., Petrycki, E.R., 2011. An igneous origin for Rima Hyginus and Hyginus Crater on the Moon. Icarus 215, 584–595.
Wolfe, E.W., Morris, J., 1996. Geologic Map of the Island of Hawai'i. *U.S. Geological Survey Miscellaneous Investigations Series* I–2524-A scale 1:100,000.
Wyrick, D., Ferrill, D.A., Morris, A.P., Colton, S.L., Sims, D.W., 2004. Distribution, morphology, and origins of Martian pit crater chains. J. Geophys. Res. B 109 (E6). https://doi.org/10.1029/2004/JE002240.